Cell Reports

Article

Dynamic chromatin remodeling in cycling human endometrium at single-cell level

Graphical abstract

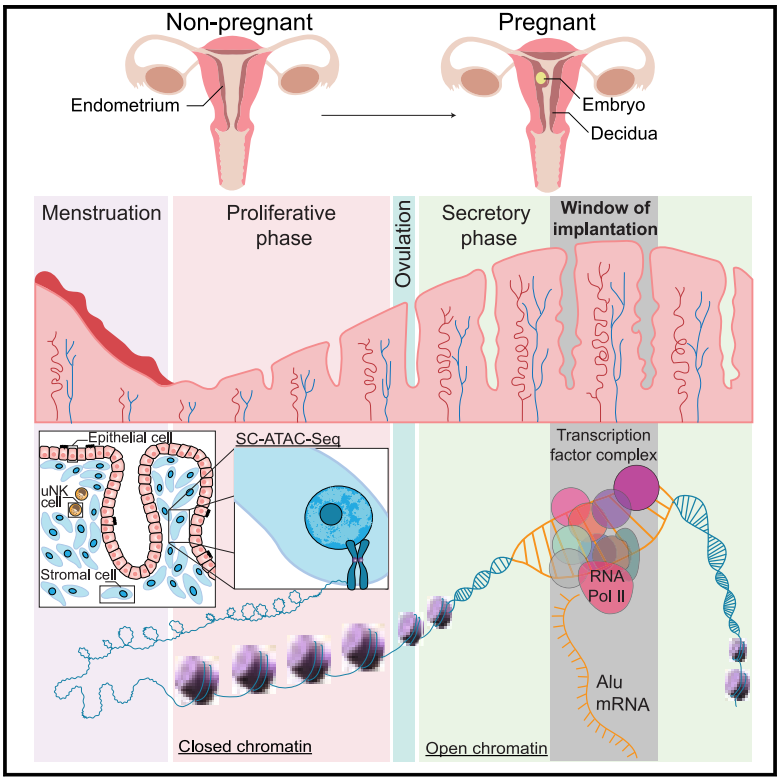

Highlights

- Temporal changes in chromatin accessibility in endometrial cells span the menstrual cycle
- Access to regulatory DNA elements coordinates cycle-dependent gene expression
- Implantation window linked to cooption and transcription of transposable elements

Authors

Pavle Vrljicak, Emma S. Lucas, Maria Tryfonos, Joanne Muter, Sascha Ott, Jan J. Brosens

Correspondence

j.j.brosens@warwick.ac.uk

In brief

Vrljicak et al. use scATAC-seq to investigate cycle-dependent gene expression in the human endometrium, uncovering that temporal chromatin changes coordinate transcription factor access to enriched *cis*-regulatory DNA elements. Opening of the implantation window coincides with sequential cooption of old and young transposable elements into the regulatory chromatin landscape of decidualizing cells.

Vrljicak et al., 2023, Cell Reports *42*, 113525
December 26, 2023
https://doi.org/10.1016/j.celrep.2023.113525

CellPress

Cell Reports

CellPress
OPEN ACCESS

Article

Dynamic chromatin remodeling in cycling human endometrium at single-cell level

Pavle Vrljicak,[1,2] Emma S. Lucas,[1] Maria Tryfonos,[1] Joanne Muter,[1,3] Sascha Ott,[1,2] and Jan J. Brosens[1,3,4,*]
[1]Warwick Medical School, Division of Biomedical Sciences, University of Warwick, Coventry CV2 2DX, UK
[2]The Zeeman Institute for Systems Biology and Infectious Disease Epidemiology Research (SBIDER), University of Warwick, Coventry CV4 7AL, UK
[3]Tommy's National Centre for Miscarriage Research, University Hospitals Coventry & Warwickshire NHS Trust, Coventry CV2 2DX, UK
[4]Lead contact
*Correspondence: j.j.brosens@warwick.ac.uk
https://doi.org/10.1016/j.celrep.2023.113525

SUMMARY

Estrogen-dependent proliferation followed by progesterone-dependent differentiation of the endometrium culminates in a short implantation window. We performed single-cell assay for transposase-accessible chromatin with sequencing on endometrial samples obtained across the menstrual cycle to investigate the regulation of temporal gene networks that control embryo implantation. We identify uniquely accessible chromatin regions in all major cellular constituents of the endometrium, delineate temporal patterns of coordinated chromatin remodeling in epithelial and stromal cells, and gain mechanistic insights into the emergence of a receptive state through integrated analysis of enriched transcription factor (TF) binding sites in dynamic chromatin regions, chromatin immunoprecipitation sequencing analyses, and gene expression data. We demonstrate that the implantation window coincides with pervasive cooption of transposable elements (TEs) into the regulatory chromatin landscape of decidualizing cells and expression of TE-derived transcripts in a spatially defined manner. Our data constitute a comprehensive map of the chromatin changes that control TF activities in a cycling endometrium at cellular resolution.

INTRODUCTION

In humans and other simians, the uterine mucosa—endometrium—is subjected to iterative cycles of menstrual breakdown and repair.[1] In each ovulatory cycle, menstrual repair is followed by rapid proliferation of resident epithelial and stromal cells in response to rising ovarian estradiol production. Proliferation in human endometrium peaks around day 10 of the cycle and leads to the formation of a superficial layer,[2] which on average quadruples the thickness and volume of the endometrium.[3] Following ovulation, proliferation in glandular epithelium first decreases and then ceases altogether, reflecting a switch in ovarian hormone production to progesterone. The onset of apocrine glandular secretion coincides with an abrupt change in gene expression,[4] indicative of an epithelial cell stress response that marks the start of the mid-secretory implantation window.[5,6] An acute stress response, termed "decidual reaction," is also apparent in the stroma, characterized histologically by transient edema, angiogenesis, and influx and proliferative expansion of uterine natural killer (uNK) cells.[1,6] In parallel, inflammatory reprogramming of stromal cells over approximately 4 days leads to the emergence of stress-resistant, progesterone-dependent decidual cells, heralding closure of the implantation window.[7] Upon embryo implantation, sustained progesterone signaling enables decidual cells to engage uNK cells, resulting in pruning of stressed and senescent fibroblasts and transformation of the endometrium into the decidua of pregnancy,[7–9] a tolerogenic matrix in which local immune cells cooperate with invading placental trophoblast to form a hemochorial placenta.[10,11] In non-conception cycles, however, decidual cells switch to a senescent phenotype in response to falling progesterone levels, triggering sterile inflammation, influx of neutrophils and macrophages, tissue breakdown, and menstrual shedding of the superficial endometrial layer.[1]

Ovarian hormones exert overall control over endometrial dynamics across the menstrual cycle through binding and activation of their cognate nuclear receptors in resident stromal and epithelial cells. The estrogen receptor 1 (ESR1) and progesterone receptor (PGR) isoforms PGR-A and PGR-B (encoded by a single gene, *PGR*) are members of the nuclear receptor superfamily of transcription factors (TFs). Upon activation, the receptors dimerize, bind canonical DNA response elements in promoter or distal enhancer regions of target genes, and recruit cofactors and coregulators (i.e., coactivators and corepressors) to activate or silence gene expression.[12] Estrogen-dependent proliferation of the endometrium is spatially restricted and becomes more pronounced with increasing distance away from the basal layer, likely reflecting the presence of morphogen and cytokine gradients involved in tissue patterning and cell specification.[1] Following ovulation, progesterone-dependent differentiation is restricted to the superficial layer and mediated by complex local autocrine and paracrine signals, induction of

evolutionarily conserved TFs, and sequential activation of cell-specific gene networks.[6,7] Approximately 5 days after ovulation, the endometrium becomes receptive to embryo implantation. Timing of the implantation window is critical as it aligns embryonic development to the blastocyst stage with a maternal environment supportive of post-implantation development. Consequently, asynchronous embryo implantation is considered a major cause of infertility and early pregnancy loss,[13] although the underlying pathological mechanisms remain poorly understood.

How the myriad of hormone-dependent signals and effectors are integrated to produce cell-specific and time-sensitive transcriptional responses is a major unresolved issue in endometrial biology. Endometrial differentiation coincides with altered histone modifications and other epigenetic changes,[6,14,15] which control chromatin structure, that is, packaging of genomic DNA into nucleoprotein complexes. The epigenetic landscape, which organizes the chromatin into sites of accessible and restricted DNA, is cell specific and highly dynamic, with structural transitions reportedly occurring on timescales that range from milliseconds to minutes and hours.[16] Thus, the ability of TFs and cofactors to regulate gene expression is spatiotemporally constrained by accessibility to specific *cis*-regulatory elements in promoter and enhancer regions. In this study, we subjected timed endometrial biopsies to single-cell assay for transposase-accessible chromatin with sequencing (scATAC-seq).[17] We demonstrate that endometrial differentiation is underpinned by coordinated "waves" of chromatin remodeling that demarcate networks of accessible sites enriched in specific TF binding sites (TFBSs). Further, dynamic changes in chromatin accessibility span the entire secretory phase of the menstrual cycle and lead to cooption of transposable elements (TEs), including Alu, LINE-1 (L1), and other elements, into the regulatory landscape of decidualizing stromal cells during the implantation window. Thus, dynamic changes in chromatin accessibility codify the multitude of signals implicated in cyclical endometrial remodeling into robust hormone-dependent gene expression programs.

RESULTS

Identification of endometrial cell types by scATAC-seq

Flash frozen endometrial biopsies obtained on different days of the menstrual cycle were subjected to scATAC-seq (Figure 1A). Demographic information on study participants and quality control of the scATAC-seq data are presented in Table S1A. Proliferative phase endometrial biopsies were timed relative to the start day of menstruation (n = 2, designated P7 and P10), whereas secretory phase samples were obtained on different days following the pre-ovulatory luteinizing hormone (LH) surge as determined by home ovulation testing. Each secretory phase biopsy was assigned the equivalent day of a standardized 28-day cycle (n = 10, designated S18–S25). To ensure accurate timing of the post-ovulatory biopsies, transcript levels of two epithelial genes, *GPX3* and *SLC15A2*, were measured (Table S1A). *GPX3* and *SLC15A2* are up- and downregulated, respectively, upon progression of the secretory phase,[18] making the ratio of expression levels a convenient marker of "endometrial time." Further, two biopsies each were obtained on cycle days 19 and 21 (S19/S19a and S21/S21a) and were included as timing controls.

A total of 36,177 nuclei passed quality control (Table S1A). Following clustering and UMAP (uniform manifold approximation and projection) dimensionality reduction, six major cell clusters with unique patterns of accessible chromatin were identified (Figures 1B and 1C). Cross-referencing of inferred gene expression levels based on chromatin accessibility with known marker genes of endometrial cell types (GEO: GSE127918, Table S1B)[7] readily identified the clusters as stromal cells (SCs; ~46.6% of total nuclei), epithelial cells (EpCs; ~44.4%), ciliated epithelial cells (cEpCs; ~1.2%), endothelial cells (ECs; ~1.2%), and two major immune cell populations (IC1, ~4.8%, and IC2, ~1.8%), corresponding to uNK cells and monocytes/macrophages, respectively (Figure 1D).[7] Evidence of temporal changes in chromatin accessibility in stromal and epithelial cells was obvious from UMAP visualization, with pre- and post-ovulatory populations forming distinct clusters and the appearance of a gradient based on timing of samples across the secretory phase of the cycle. Further, the chromatin accessibility profiles of samples obtained on the same menstrual cycle day (S19/S19a and S21/S21a) aligned closely.

Transition from the proliferative to secretory endometrium

The ovulatory shift in ovarian hormone production from estradiol to progesterone controls the transition from proliferative to secretory endometrium. A comparison of scATAC-seq profiles between proliferative and secretory endometrial biopsies identified 5,101 dynamic chromatin regions in epithelial cells (Table S2A). With 2,146 differentially accessible regions (Table S2A), the genomic response to the change in hormonal environment was less pronounced in stromal cells. Proportionally more loci closed than opened upon transition to secretory phase of the cycle in both cell types (epithelial cells: 3,989 vs. 1,099; stromal cells: 1,575 vs. 571, respectively). Dynamic loci in stromal and epithelial cells overlapped with putative binding sites for ESR1 and PGR, termed estrogen- and progesterone-response elements (ERE and PRE, respectively) (Figure 2A). Compared to all accessible chromatin regions, dynamic loci in stromal and epithelial cells were highly enriched in putative binding sites for EREs, independent of the cycle phase. Chromatin regions that became accessible following ovulation were further enriched in PREs without a reciprocal loss of putative EREs. Thus, ESR1 and PGR likely play a role in regulating endometrial gene expression in both phases of the menstrual cycle, in keeping with previous studies demonstrating ligand-independent activity of these nuclear receptors.[19,20] In the case of PRE, it should be noted that this response element can potentially also bind other nuclear receptor subfamily 3 group C (NR3C) members, including the androgen receptor (AR), glucocorticoid receptor (NR3C1), and mineralocorticoid receptor (NR3C2). Next, we subjected temporally regulated chromatin regions to *de novo* motif enrichment analysis to identify TFs involved in proliferative to secretory phase transition. In epithelial cells, ATAC-seq peaks that closed following ovulation were highly enriched ($p < 10^{-85}$, binomial test) in a motif best matched by

CellPress
OPEN ACCESS

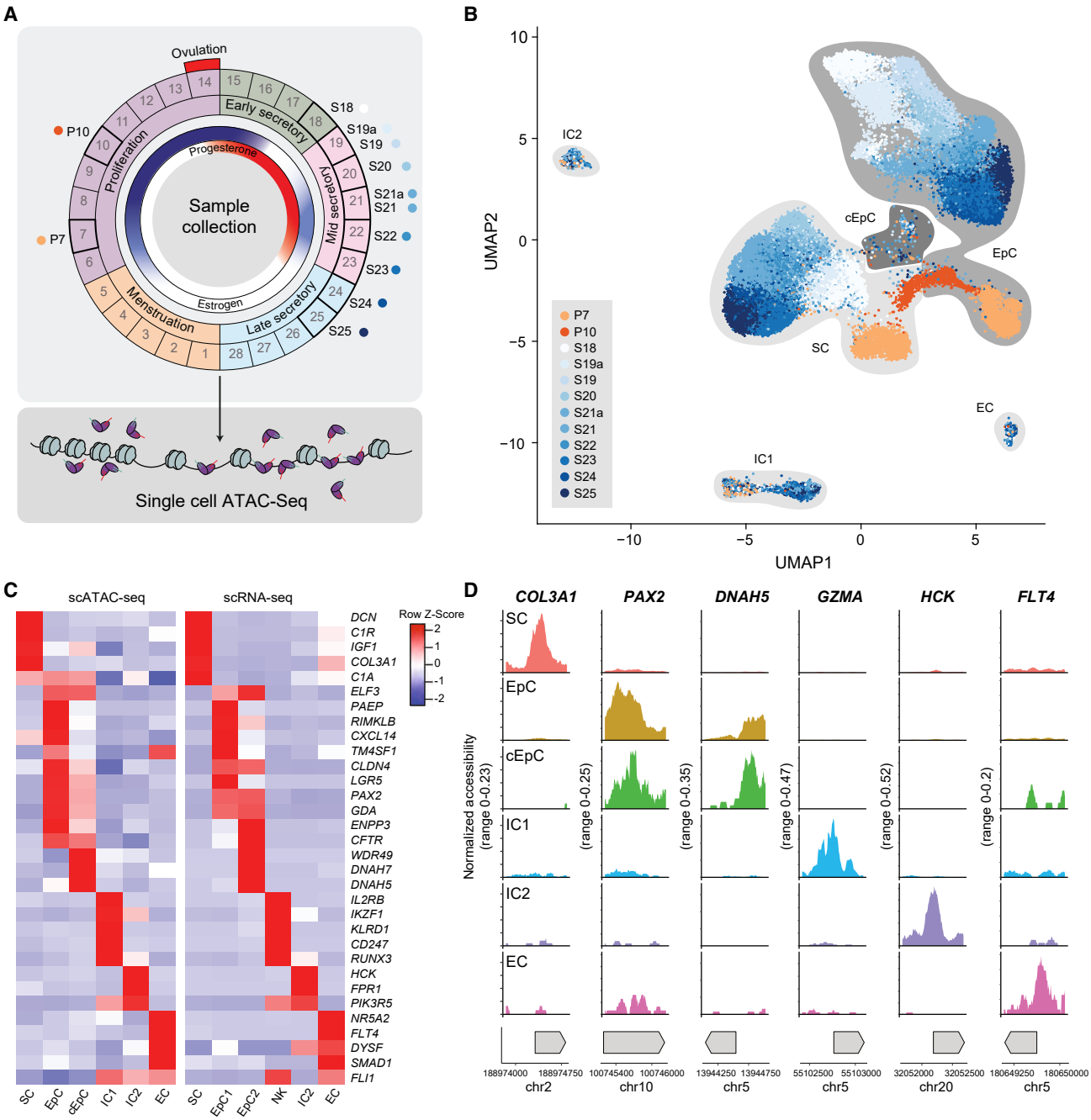

Figure 1. scATAC-seq analysis of cycling human endometrium

(A) Schematic illustrating the menstrual cycle, ovarian hormone levels, and day of endometrial sample collection. Proliferative samples (n = 2) were collected at 7 and 10 days (P7 and P10) after the start of the last menstrual period. Secretory samples (n = 10) were obtained 5 to 12 days following the pre-ovulatory LH surge and designated the equivocal day of a standardized 28-day cycle (S18–S25). Two biopsies were obtained on cycle days 19 (S19/19a) and 21(S21/21a).

(B) Endometrial cell clusters from ATAC-seq analysis were visualized by UMAP and colored by the cycle day of samples. A total of 36,177 nuclei were analyzed. Cell types were identified as stromal cells (SCs, n = 16,851 nuclei), endothelial cells (ECs, n = 435), immune cells (IC1s and IC2s; n = 1,741 and n = 645, respectively), and unciliated epithelial cells (EpCs, n = 16,075) and ciliated EpCs (cEpCs, n = 430).

(C) Heatmap showing cell-type-specific inferred RNA expression (*Z* score) by scATAC-seq and expression of corresponding transcripts in scRNA-seq data from six endometrial biopsies. The scRNA-seq data were extracted from the study of Lucas et al.[7]

(D) Examples of differential accessibility to regulatory chromatin regions at canonical marker genes in different endometrial cell types.

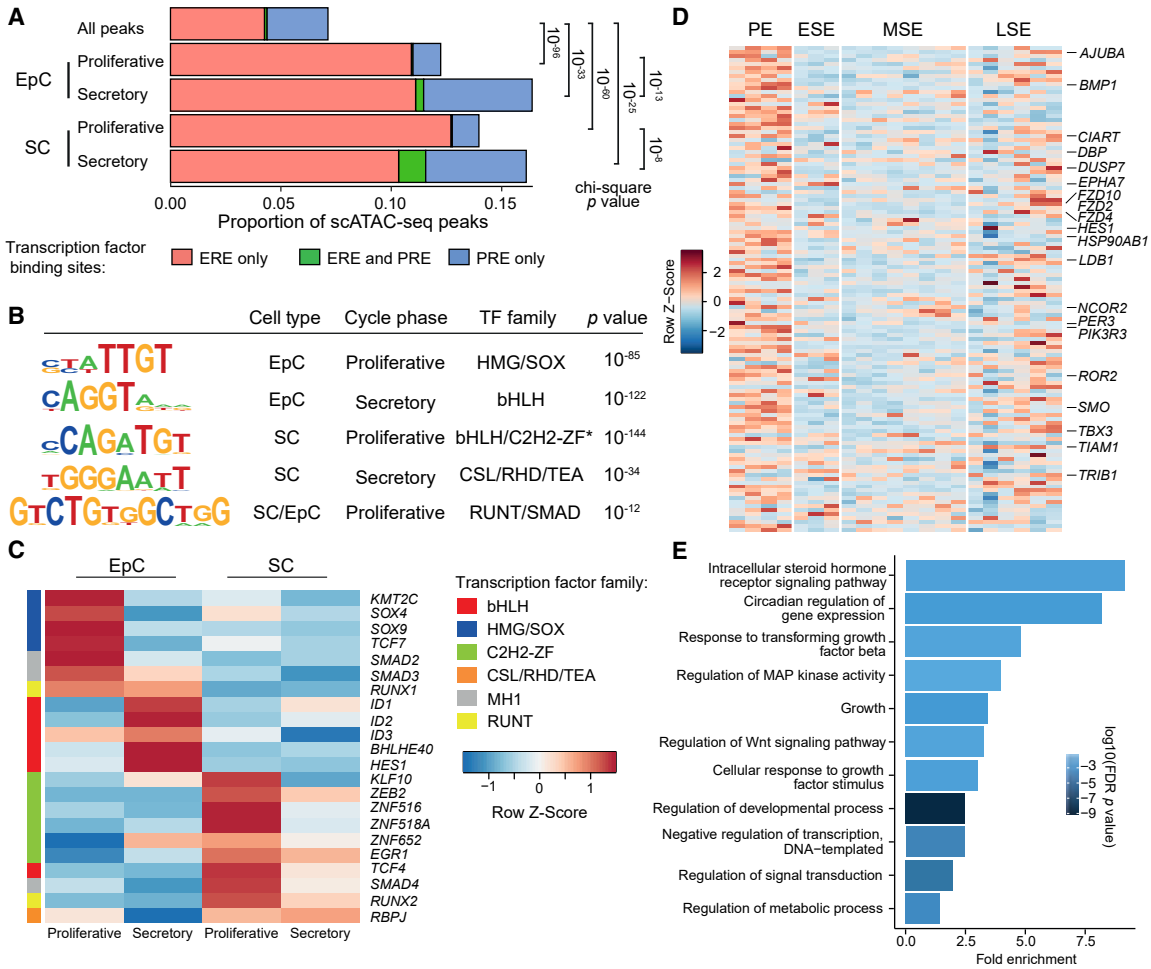

Figure 2. Chromatin accessibility in stromal and epithelial cells during the proliferative and secretory phase of the cycle

(A) Enrichment of ESR and PGR binding sites (EREs and PREs, respectively) in proliferative and secretory epithelial and stromal cells (EpCs and SCs, respectively). "All peaks" refers to every ATAC-seq peak in our dataset.

(B) TF binding motifs enriched in opening and closing chromatin regions in proliferative versus secretory phase endometrium. p values represent binomial test results using HOMER.[23] Best TF family matches were based on known motifs in the HOMER motif database (Table S1C). * indicates statistically significant TF family matches (FDR corrected $p < 0.05$).

(C) Heatmap showing relative mRNA expression (*Z* score) in EpCs and SCs of candidate TFs in proliferative and secretory endometria. The scRNA-seq data on 10 endometrial samples were extracted from the study of Wang et al.[4]

(D) Heatmap showing relative RNA expression (*Z* score) of nearest gene to each closing chromatin region in bulk gene expression data from 21 endometrial samples obtained across the menstrual cycle. The data were extracted from the study of Talbi et al.[22] PE, proliferative endometrium (n = 4); ESE, early-secretory endometrium (n = 3); MSE, mid-secretory endometrium (n = 8); LSE, late-secretory endometrium (n = 6).

(E) Gene Ontology analysis of genes silenced upon ovulation near closing chromatin loci in both stromal and epithelial cells.

high-mobility group (HMG)/SOX TFBSs, whereas binding motifs best matched to basic-helix-loop-helix (bHLH) TFBSs were overrepresented in opening peaks ($p < 10^{-122}$, binomial test) (Figure 2B). Cross-referencing with published scRNA-seq data (GEO: GSE111976, Table S1B)[4] identified several highly expressed members of the HMG/SOX and bHLH TF families with temporal expression profiles that match the switch in TFBSs in dynamic chromatin regions (Figure 2C; Table S2B). By contrast, accessible loci restricted to proliferative stromal cells harbored an abundance of Cys2-His2 zinc finger (C2H2-ZF) TFBS ($p < 10^{-144}$, binomial test) (Figure 2B). Repression of these sites following ovulation, and loss of corresponding TFs (Figure 2C), coincided with gain of binding sites best matching the transcriptional regulator RBPJ motif ($p < 10^{-34}$, binomial test), which functions as transcriptional repressor in the absence of Notch signaling and an activator when bound to Notch proteins.[21] Interestingly, 262 genomic regions closed following ovulation in both epithelial and stromal cells (Table S2A). These regions were enriched in binding sites best matching RUNT/SMAD TFBSs ($p < 10^{-12}$, binomial test) (Figures 2B and 2C). Expression analysis of the nearest gene to each closing peak in whole tissue samples (GEO: GSE4888, Table S1B)[22] showed a biphasic response, characterized by rapid downregulation in early-secretory endometrium followed by loss of repression prior to

menstruation (Figure 2D), reflecting the rise and fall in circulating progesterone levels, respectively. Further, Gene Ontology analysis revealed that genes near chromatin that closes following ovulation in both the stromal and epithelial compartments are implicated in various signal transduction pathways (WNT, TGF-β, MAPK, and steroid hormone signaling) and key biological processes (e.g., growth, metabolism, and circadian gene regulation) (Figure 2E).

Dynamic chromatin changes in differentiating epithelial cells

Next, we set out to map the temporal changes in chromatin accessibility across the implantation window in epithelial cells. The endometrium becomes receptive 5 days after ovulation for approximately 4 days (S19–S22). First, we performed pairwise comparisons of scATAC-seq peaks in epithelial cells from samples obtained between S18 and S25 to identify dynamic chromatin loci. The resulting 8,217 chromatin regions were then grouped in three temporal patterns using k-means clustering (Figure 3A; Table S3A). Pattern 1 represents 4,624 dynamic loci that close during the implantation window in a coordinated manner. Patterns 2 (n = 1,645) and 3 (n = 1,948) capture chromatin regions that open during the implantation window, and they either remain stable or open further upon transition to the late-secretory phase of the cycle, respectively. Cross-referencing with bulk endometrial gene expression data spanning the menstrual cycle (GEO: GSE4888, Table S1B)[22] revealed that epithelial genes near closing chromatin loci in pattern 1 are downregulated in mid-secretory endometrium, whereas comparable genes in patterns 2 and 3 are induced (Figure S1). While pattern 2 genes tend to peak during the mid-secretory implantation window, the expression of pattern 3 genes is maintained or enhanced upon transition to the late-secretory phase (Figure S1).

We subjected the dynamic chromatin loci in patterns 1–3 to *de novo* motif enrichment analysis, repeating the analysis five times with shuffled chromatin regions to establish a robust threshold for statistical significance for each pattern (see STAR Methods). A total of 11 significant motifs were identified, eight in pattern 1 (designated P1M1-8), one in pattern 2 (P2M1), and two in pattern 3 (P3M1-2) (Figure S2A). Based on evidence of a temporal pattern in footprint analysis (Figure S2B) and enrichment over all ATAC-seq genomic regions (Figures S2C and S2D), seven of the 11 overrepresented motifs were deemed bona fide *cis*-regulatory elements involved in coordinated chromatin remodeling in epithelial cells across the implantation window (Figure 3B). Chromatin regions that close during the implantation window (pattern 1) were highly enriched for HMG/SOX TFBSs ($p < 10^{-274}$, binomial test, Figure 3B), continuing the trend observed upon transition from proliferative to secretory phase of the cycle (Figure 2B). Other closing loci in pattern 1 harbored motifs best matched by Forkhead and C2H2-ZF TFBSs ($p < 10^{-57}$ and $p < 10^{-48}$, binomial test, respectively) as well as putative steroid hormone receptors (NR3C, $p < 10^{-48}$ and $p < 10^{-48}$, binomial test) (Figure 3B). Among the epithelial chromatin regions that open during the implantation window, pattern 2 loci were highly enriched for bZIP TFBSs ($p < 10^{-205}$, binomial test), whereas homeobox TF binding motifs were overrepresented in pattern 3 ($p < 10^{-100}$, binomial test). We noted that several cycle-dependent endometrial TFs possess dynamic TF binding motifs in their regulatory regions (Table S3B). For example, the closing chromatin locus upstream of *SOX17*, an epithelial cell-enriched TF, contains an HMG/SOX binding motif (Figure 3C), thus implicating SOX17 in its own regulation. Next, we compiled a set of TFs that potentially engage enriched TF binding motifs in pattern 1–3 based on their level and temporal pattern of expression in RNA-seq data of laser-dissected endometrial glands (GEO: GSE84169, Table S1B)[24] obtained before (S18), during (S21), and after (S24) the implantation window (Figure 3D; Table S3C). For example, *HNF1B* is the highest expressed homeobox TF gene in glandular epithelium with a temporal expression profile that follows pattern 3 closely. Immunohistochemistry of timed endometrial biopsies confirmed that the increase in HNF1B expression in glandular epithelium during the window of implantation is maintained upon transition to the late-secretory phase (Figures 3E and 3F).

Ciliated cells made up approximately 2.7% of the captured epithelial cell fraction in our ATAC-seq dataset. While the epigenetic landscape of ciliated epithelial cells is distinct, it is not subjected to obvious temporal changes across the menstrual cycle (Figure 1B). When compared to their unciliated counterparts, accessible chromatin regions in ciliated cells were enriched in five TF binding motifs, most prominently for the regulatory factor X (RFX) family of TFs ($p < 10^{-58}$, binomial test, Figure S4A). Two family members, RFX2 and RFX3, are direct regulators of core cileogenic genes and expressed selectively in endometrial ciliated epithelial cells.[25] Figure 3G shows examples of RFX binding sites in proximity of genes (*LDLRAD1*, *AK8*, and *SPACA9*) involved in cilia assembly.[26]

Dynamic chromatin changes in decidualizing stromal cells

The mid-secretory implantation window coincides with decidualization, a process defined by inflammatory reprogramming of stromal cells into specialized decidual cells.[1,6] The emergence of phenotypic decidual cells on day 23 (S23) of a standardized 28-day cycle, characterized by their rounded appearance and enlarged nuclei, marks the closure of the window.[5] Using the same approach as for epithelial cells, we resolved the 2,392 dynamic chromatin loci in stromal cells between S18 and S25 into four temporal patterns (patterns 1–4, Figure 4A; Table S4). Chromatin dynamics in decidualizing stromal cells were notably more variable when compared to differentiating epithelial cells, likely reflecting that endometrial glands are clonal in origin and therefore subject to tighter regulatory control.[27] Opening of the implantation window was marked by a sequential shift in peak accessibility from pattern 1 to patterns 2 and 3, whereas closure of the window coincided with maximal accessibility in pattern 4. Using *de novo* motif analysis, we identified 16 significantly overrepresented TF motifs across the four patterns (Figure S3A), 12 of which were considered primary *cis*-regulatory elements based on the presence of a temporal pattern in footprint analysis (Figure S3B) and enrichment over all ATAC-seq genomic regions (Figures 3D and S3C). As shown in Figure 4B, patterns 1 and 4, which mark the boundaries of the implantation window, were selectively enriched in C2H2-ZF and bZIP TFBSs, respectively. Multiple motifs were overrepresented in patterns 2 and 3, likely reflecting active reprogramming of stromal cells into pre-decidual cells. Next we

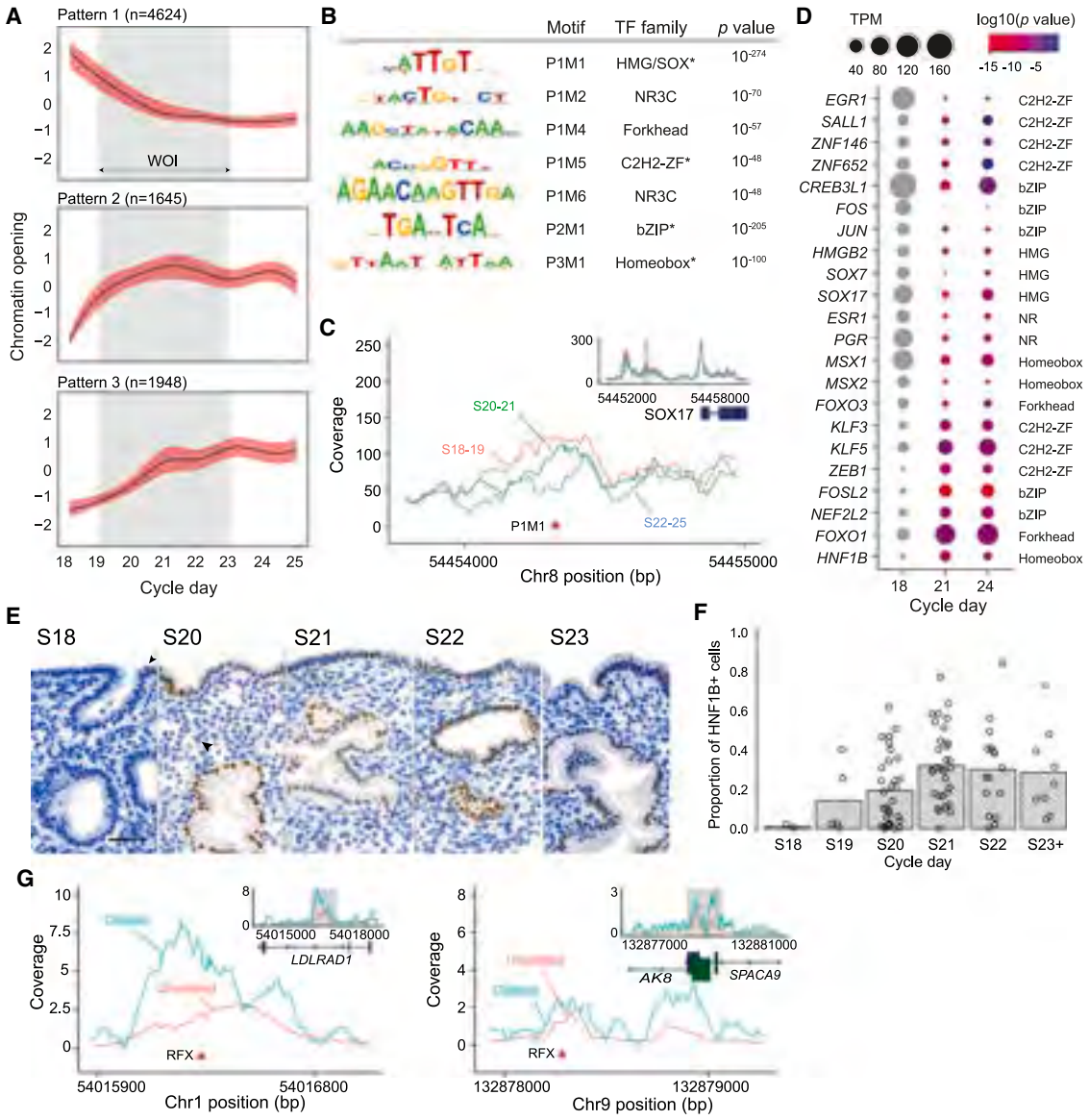

Figure 3. Dynamic chromatin remodeling in secretory phase epithelial cells

(A) Clustering of dynamic chromatin loci in secretory phase epithelial cells into three temporal patterns (patterns 1–3). The number of peaks in each pattern is indicated in the figure. Trend curve represents locally estimated scatterplot smoothing (LOESS) fit ± standard error (red). The shaded area demarcates the putative implantation window (WOI).

(B) TF binding motifs enriched in temporally regulated genomic regions from (A) (designated as P1M1 for pattern 1 motif 1, etc.). p values represent binomial test results using HOMER.[23] Only motifs with temporal pattern footprint analysis and enrichment over all ATAC-seq genomic regions are shown. Best TF family matches were based on known motifs in the HOMER motif database (Table S1C). * indicates statistically significant TF family matches (FDR corrected $p < 0.05$).

(C) Cycle-dependent changes in chromatin accessibility upstream of *SOX17*. The location of an HMG/SOX binding site (P1M1) is indicated.

(D) Expression of candidate TFs before (S18), during (S21), and after (S24) the implantation window. The data were obtained from RNA-seq analysis of laser-captured endometrial glands,[24] expressed as transcripts per million (TPM; Table S3), and p values are based on expression on day 21 (S21, n = 3) and day 24 (S24, n = 3) versus day 18 (S18, n = 3) (Wald test using DESeq2).

(E) HNF1B immunoreactivity in secretory phase endometrium. Arrows show nuclear HNF1B staining (brown). The scale bar denotes 100 μm.

(F) Proportion of HNF1B-positive cells in endometrial glands across the peri-implantation window. Immunohistochemistry was performed on 96 timed endometrial samples.

(G) Examples of differential chromatin accessibility in ciliated versus unciliated epithelial cells. Locations of RFX binding motifs are shown.

mined scRNA-seq data (GEO: GSE111976, Table S1B)[4] to identify TFs in stromal cells that are temporally regulated across the peri-implantation window. In keeping with our scATAC-seq data, several genes encoding for C2H2-ZF TFs of the Krüppel-like factor (KLF) family (pattern 1) are downregulated upon opening of the implantation window, which is followed by induction of genes

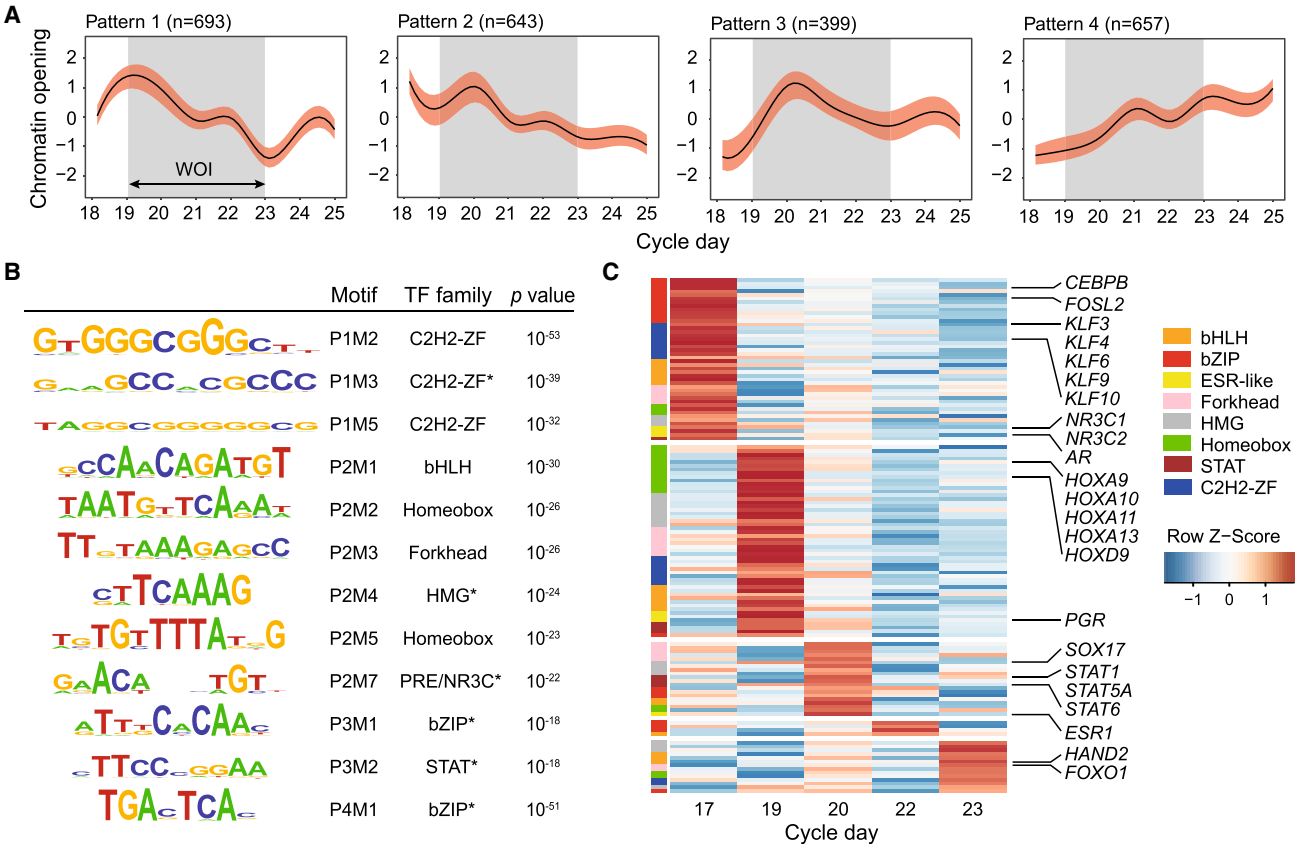

Figure 4. Dynamic chromatin remodeling in secretory phase stromal cells

(A) Clustering of dynamic chromatin loci in secretory phase stromal cells into four temporal patterns (patterns 1–4). The number of peaks in each pattern is indicated in the figure. Trend curves represents LOESS fit ± standard error (red). The shaded area demarcates the putative implantation window (WOI).

(B) TF binding motifs enriched in temporally regulated genomic regions from (A) (designated as P1M1 for pattern 1 motif 1, etc.). p values represent binomial test results using HOMER.[23] Only motifs with temporal pattern in footprint analysis and enrichment over all ATAC-seq genomic regions are shown. Best TF family matches were based on known motifs in the HOMER motif database (Table S1C). * indicates statistically significant TF family matches (FDR corrected $p < 0.05$).

(C) Relative expression (*Z* score) of candidate TFs. The data were extracted from the study of Wang et al.[4] See also Table S4.

encoding known core TFs in pre-decidual cells, including HOXA (homeobox A cluster, pattern 2) and STAT (signal transducer and activator of transcription) family members (pattern 3) (Figure 4C).[28,29] Notably, pattern 2 is also enriched in NR3C binding sites. Apart from estradiol and progesterone, decidualizing stromal cells are responsive to androgen and corticosteroid signaling, at least in primary cultures.[19,30] In line with these observations, all steroid hormone receptor (NR3C) genes (*ESR1*, *PGR*, *AR*, *NR3C1*, and *NR3C2*) are dynamically expressed in pre-decidual cells across the implantation window *in vivo* (Figure 4C). Thus, a notable level of congruency was observed between accessibility to TFBSs in patterns 1–3 and the temporal expression of corresponding TFs. However, congruency was less obvious for pattern 4, which captures the dynamic chromatin regions in emerging decidual cells around day 23 of a standardized 28-day cycle.

Cooption of transposable elements during the implantation window

Novel *cis*-regulatory elements encoded by mammalian-, therian-, and eutherian-specific TEs played an important role in the emergence of decidual cells in ancestral eutherian (placental) mammals.[31,32] A second wave of TE cooption in catarrhine primates (Old World monkeys, apes, humans) has been linked to the emergence of novel reproductive traits, such as spontaneous decidualization of the endometrium (i.e., independently of embryo implantation) and menstruation.[33] To gain insights in the regulation of decidualizing stromal cells, we mapped enriched TEs across all the temporal scATAC-seq peaks. We expanded this set by including scATAC-seq peaks with similar temporal patterns (Figure S3C) that did not meet our initial stringent criteria for temporal regulation. Progressive differentiation of stromal cells into pre-decidual (pattern 3) and decidual cells (pattern 4) coincided with repression of low-complexity elements and simple repeats and enrichment of distinct TE families across the five major classes: DNA transposons, short interspersed nuclear elements (SINEs), long interspersed nuclear elements, composite SVA (SINE-VNTR-Alus) elements, and long terminal repeats retrotransposons (Figure 5A; Table S5). Intriguingly, when compared to pre-decidual cells (pattern 3), accessible chromatin loci in decidual cells (pattern 4) are characterized by overdispersion of

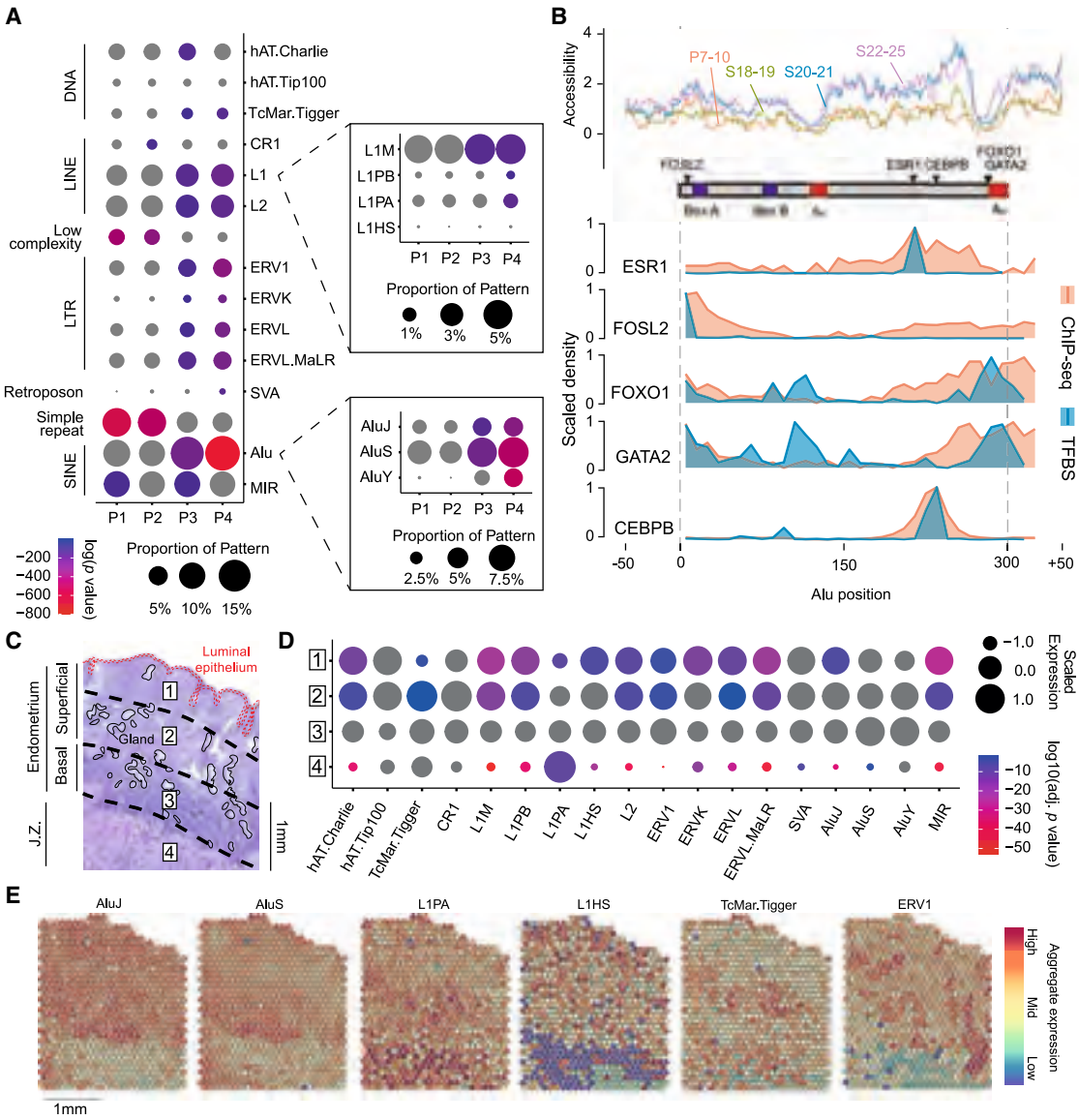

Figure 5. Transposable elements in dynamic chromatin regions in decidualizing stromal cells

(A) Enrichment of transposable elements (TEs) in the temporal chromatin waves in decidualizing stromal cells. Temporal patterns represent expanded set of peaks with high similarity to sets in Figure 4A. The size of the circles denotes the proportion of TEs, and the color key indicates p values (hypergeometric test for enrichment).

(B) Analysis of Alu element showing boxes A and B (blue) and A-rich regions (red). Cycle-dependent changes in chromatin accessibility are color coded and labeled by the cycle day of the sample. Scaled density plots showing location of predicted and validated TFBSs from JASPAR database and ChIP-seq peak summits, respectively.

(C–E) Spatial transcriptomic analysis of an early-secretory phase full-thickness endometrial sample with adjacent junctional zone myometrium.[41] (C) Hematoxylin and eosin (H&E) staining of the tissue sample. For transcriptomic analysis, the sample was divided into four regions, broadly corresponding to the superficial endometrial layer (regions 1 and 2), the regenerative basal layer (region 3), and junctional zone myometrium (region 4). (D) Normalized average expression of TE-derived transcripts across the four regions. The size of the circles corresponds to the change in relative expression from the mean. The color key denotes the adjusted p value in one region against the other three regions (Wilcoxon rank-sum test). (E) Examples of spatial expression of TE-derived transcripts across the endometrium and junctional zone myometrium.

evolutionarily young TE families and subfamilies (e.g., SVA, L1PA, and AluY) and loss of some older elements (e.g., MIR and hAT.Charlie) (Figure 5A). Perhaps the most salient feature of decidualizing stromal cells is the cooption of primate specific Alu elements, which make up ~11% of the human genome. Compared to scATAC-seq peaks in stromal cells (pattern 1), enrichment in decidual cells (pattern 4) was 1.53-fold for AluJ, the oldest of the Alu lineages, 1.52-fold for AluS, and 3.15-fold for AluY, the youngest lineage which expanded in catarrhine primates.[34] Alu elements are 300 bp in length and composed of a left and right

monomer on either side of an A-rich linker region and a 3′ poly-A tail. The A and B boxes in the left monomer contain RNA polymerase III promoter binding sites. In decidualizing stromal cells, accessibility to Alu elements increases in a time-dependent manner (Figure 5B). Integrative analysis of putative *cis*-regulatory elements and chromatin immunoprecipitation sequencing (ChIP-seq) data obtained from primary endometrial stromal cell cultures[35–38] and the ENCODE database[39] confirmed binding of decidual TFs, including GATA2, FOXO1, and CEBPB,[6,40] to a cluster of canonical TFBSs in the right monomer of opening *Alu* elements (Figure 5B). ChIP-seq data also demonstrated prominent binding of ESR1, although not PGR, in line with TFBS predictions (Figures 5B and S5).

Endometrial responses to steroid hormone signaling are spatially organized and largely confined to the superficial endometrium.[1] Hence, we examined the expression of TE-derived transcripts in spatial transcriptomic data (Visium) on a hysterectomy specimen obtained in the early secretory phase of the menstrual cycle (ArrayExpress: E-MTAB-9260; 152807, Table S1B)[41] and comprising full-thickness endometrium and adjacent myometrium, also termed "junctional zone" myometrium. We used a modified pipeline to count TE-derived reads in a locus-specific manner across four zonal uterine regions (Figure 5C).[42] Regions 1 and 2 represent the superficial endometrial layer, whereas regions 3 and 4 capture broadly the basal endometrial layer and junctional zone myometrium, respectively (Figure S6A). As shown in Figures 5D and 5E, TE-derived transcripts, with exception of L1PA, are more abundantly expressed in the endometrium than junctional zone myometrium. However, L1HS (previously known as L1PA1), the evolutionarily youngest and the only active L1 subfamily in the human genome,[43] is expressed most prominently in subluminal endometrium. Further, even within the superficial endometrium (regions 1 and 2), there was evidence of a gradient in the expression of TE-derived transcripts (Figures 5D and 5E). To substantiate these observations, we measured the expression of L1 and Alu mRNA in 36 RNA-seq libraries derived from endometrial biopsies obtained between days 18 and 25 of the cycle.[18] L1 RNA is bicistronic, encoding two non-overlapping open reading frames, ORF1 and ORF2, whose protein products (ORF1p and ORF2p) bind L1 RNA to form a ribonucleoprotein complex.[44] Interestingly, principal component 3 (PC3), which accounted for 6.64% of gene variance in this set of 36 endometrial samples, correlated closely with the expression of Alu and L1 transcripts ($R^2 = 0.72$, $p = 8.2 \times 10^{-11}$ and $R^2 = 0.79$, $p = 3.2 \times 10^{-13}$, respectively) (Figure S6B). In L1 and Alu mRNA-enriched samples, PC3 was driven by genes overrepresented in ribosome assembly (false discovery rate [FDR] corrected $p = 2.4 \times 10^{-11}$), regulation of programmed cell death (FDR corrected $p = 4 \times 10^{-11}$), and regulation of immune system process (FDR corrected $p = 6.7 \times 10^{-5}$) (Figure S6C). By contrast, PC3 genes in L1 and Alu mRNA-depleted samples were implicated in the regulation of gene expression (FDR corrected $p = 1.1 \times 10^{-17}$), signal transduction (FDR corrected $p = 1.5 \times 10^{-6}$), chromatin organization (FDR corrected $p = 2.4 \times 10^{-5}$), and hormone responses (FDR corrected $p = 2.0 \times 10^{-3}$) (Figure S6C). Although only correlative, these observations nevertheless suggest an important role for TE-derived transcripts in endometrial physiology.

Endometrial endothelial and immune cell populations

The endometrium is one of few adult tissues that undergo cycles of physiological angiogenesis.[45] Although endometrial endothelial cells express ESR1 and PGR,[46] we did not observe a compelling temporal scATAC-seq signature (Figure 6A). However, vascular and lymphatic endothelial cell clusters were readily identified based on differences in chromatin accessibility (EC1 and EC2, respectively; Figure 6A). When compared to the lymphatic ATAC-seq peaks, accessible chromatin regions in vascular endothelial cells were selectively enriched in multiple motifs, including motifs best matched to bZIP ($p < 10^{-81}$, binomial test), homeobox ($p < 10^{-75}$, binomial test), and interferon-regulatory factor (IRF; $p < 10^{-68}$, binomial test) TFBSs (Figure 6B).

Uterine immune cells, especially uNK cells, play a pivotal role in endometrial remodeling before and after embryo implantation.[8,11] We identified three subsets of uNK cells, termed NK1–3, based on differences in chromatin accessibility (Figure 6C). The NK2 and NK3 subsets were prominent in the post-menstrual endometrial sample (P7), but their relative abundance appeared stable across the remainder of the cycle. By contrast, macrophages and NK1 cells were more abundant in mid- and late-secretory endometria (Figure 6D). Cross-referencing of top inferred differentially expressed TFs with their corresponding expression in scRNA-seq data obtained from immune cells at the maternal-fetal interface in early pregnancy (ArrayExpress: PRJEB28266, Table S1B)[11] confirmed that NK1 cells correspond to cytokine-producing decidual NK1 (dNK1) cells (Figure 6E). This NK subset is characterized phenotypically by cell surface expression of killer cell immunoglobulin-like receptors and the ectonucleotidase CD39 (ENTPD1).[47] NK2 cells correspond to the intermediate dNK2 subset in early pregnancy, whereas cytotoxic NK3 cells are akin to dNK3 and T cells (Figure 6E). Next, we integrated *de novo* motif enrichment analysis and TF expression profiles to gain insight into the transcriptional regulation of endometrial immune cells. We identified five TF binding motifs selectively enriched in macrophages when compared to all uNK subsets (Figure S4B). Figure 6F shows the location of the most enriched motif (ETS, designated M-M1; $p < 10^{-95}$, binomial test) in macrophages in the proximal promoter region of *CD68*, the canonical marker of human monocytes and tissue macrophages. We also identified five motifs selectively enriched in NK1 cells when compared to NK2 or NK3 subsets (Figure S4B). Figure 6F also shows the location of the most enriched motif, a RUNT binding site designated NK1-M1 ($p < 10^{-64}$, binomial test), upstream of the transcriptional start site of *GNLY*, encoding granulysin. In keeping with the level of accessibility at this locus, *GNLY* transcript levels are high, intermediate, and low in NK1, NK2, and NK3 cells, respectively.[11]

DISCUSSION

We demonstrated that all cell types in the endometrium have a distinct genomic organization that confers access to cell-specific combinations of enriched TFBSs. We also found that the

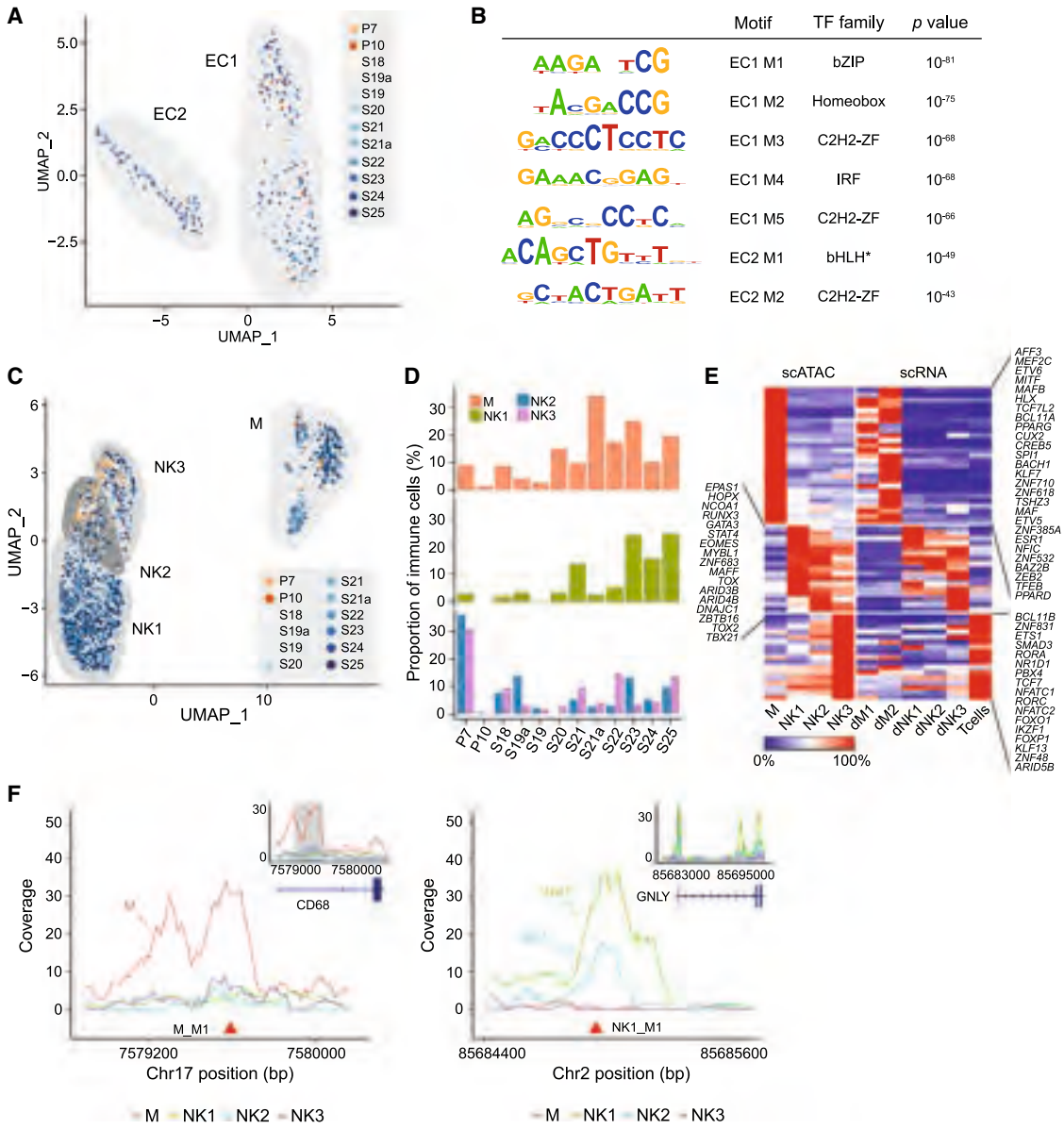

Figure 6. Chromatin accessibility in endometrial endothelial and immune cells

(A) UMAP visualization of vascular and lymphatic endothelial cells (EC1 and EC2, respectively), color coded by the day of the sample in the menstrual cycle.

(B) TF binding motifs enriched in differentially accessible chromatin regions of EC1 and EC2 nuclei. Best TF family matches were based on known motifs in the HOMER motif database (Table S1C). * indicates statistically significant TF family matches (FDR corrected $p < 0.05$).

(C) UMAP visualization of endometrial macrophages (M) and natural killer (NK) cells color coded by the cycle day of the samples.

(D) Heatmap showing relative inferred RNA expression (*Z* score) of candidate cell-type-specific TFs and expression of corresponding transcripts in scRNA-seq data. Designations of cell populations and transcript levels were extracted from the study of Vento-Tormo et al.[11]

(E) Change in immune cell subtype proportions across the secretory phase of the menstrual cycle as inferred by scATAC-seq analysis of 12 timed endometrial biopsies.

(F) Coverage plots showing differential chromatin peaks in endometrial macrophages and NK subsets. Regulatory regions of *CD68* (left) and *GNLY* (right) are shown with location of corresponding enriched TFBSs.

epigenetic landscapes of resident epithelial and stromal cells are exquisitely responsive to changes in circulating ovarian hormone levels, exemplified by the observation that many more genomic regions close than open upon transition from the proliferative to the secretory phase of the cycle. We identified a set of 262 common loci, enriched in RUNT/SMAD binding motifs, which close simultaneously in stromal and epithelial cells following ovulation. Gene Ontology analysis of the nearest genes revealed overrepresentation of modulators of multiple signal transduction pathways, including WNT and steroid hormone signaling, and core

biological processes, such as metabolism, growth, and circadian gene regulation. Despite the overall reduction in open chromatin following ovulation, access to PREs was conspicuously enriched in resident endometrial cells. Further, the emergence of a receptive endometrial state during the implantation window was underpinned by highly coordinated changes in chromatin accessibility. In epithelial cells, we discerned two distinct waves of opening chromatin, encompassing 1,645 and 1,948 loci, respectively, in parallel with loss of accessibility at 4,624 genomic sites. Similarly, decidual reprogramming of stromal cells during the implantation window involved closure of 693 genomic regions and three distinct waves of opening chromatin, each comprising hundreds of loci and peaking at different time points. The waves of opening and closing chromatin in both cell types resulted in time-sensitive enrichment and depletion, respectively, of active TFBSs as demonstrated by footprint analyses. Put differently, our findings revealed that the implantation window coincides with a coordinated switch in the regulatory DNA landscape of resident endometrial cells. To gain additional insights, we integrated our scATAC-seq findings with cell-specific and time-dependent changes in endometrial TF expression. Although this exercise does not prove that a given TF is active at a specific site, we nevertheless observed a notable degree of congruency between the gain or loss of specific *cis*-regulatory elements in dynamic chromatin regions and expression of corresponding TF family members. For example, decidual reprogramming of stromal cells during the implantation window was associated with sequential loss of C2H2-ZF motifs and enrichment of binding sites for, among others, homeobox and STAT TFs, which coincided with repression of Krüppel-like TFs and induction of known decidual transcriptional regulators, including multiple STAT and HOXA family members.[29,48,49] In epithelial cells, we identified FOSL2, an important PGR coregulator,[37] and HNF1B as putative drivers of glandular differentiation based on the alignment between expression of these TFs and enrichment of corresponding regulatory elements in opening chromatin regions.

Rapid evolution of reproductive processes in eutherians (placental mammals) is attributed to exaptation of species-specific TEs into the regulatory DNA landscape of pre-implantation embryos, placental cell lineages, and maternal decidual cells,[33,50] resulting in the gain and loss of entire gene sets between species.[51] While decidual cells likely originated in ancestral eutherians in parallel with invasive hemochorial placentation,[52] cooption of novel TE-derived *cis*-regulatory elements in catarrhine primates has been linked to the emergence of specific endometrial traits, including heightened progesterone responsiveness, spontaneous decidualization and menstruation, and deep hemochorial placentation.[33] In accordance, we observed pervasive enrichment of TEs in opening chromatin regions upon differentiation of stromal cells into pre-decidual and decidual cells, a process that marks the boundaries of the implantation window. Further, evolutionarily ancient and young TEs were coopted sequentially, indicating that decidual reprogramming of human endometrial stromal cells partly recapitulates the phylogenetic roots of this differentiation process. For example, increased accessibility to Alu elements upon differentiation of pre-decidual into decidual cells favored the relative enrichment of young (AluY) over older elements (AluS and AluJ). In line with previous observations in primary cultures,[53] exaptation of Alu elements in the regulatory DNA landscape of decidual cells enables evolutionarily core TFs, including CEBPB, FOXO1, and GATA2,[54] to access a composite response element comprising multiple TFBSs near the 3′ end of the right monomer. This observation provides further evidence that decidual gene expression is under control of multimeric TF complexes,[6,55,56] which in the case of Alu involves DNA binding of ESR1 rather than PGR.

We also demonstrated that accumulation of TE-derived transcripts is a physiological phenomenon in cycling human endometrium, especially in the decidualizing superficial layer. Retrotransposons are firmly repressed in most adult tissues because of the deleterious consequences associated with reactivation, including retrotransposition of L1 or Alu elements, genomic instability and DNA damage, transcriptional interference, and innate immune activation in response to cytoplasmic accumulation of free DNA or dsRNA.[57,58] However, de-repression of evolutionarily young retrotransposons and increased transcription are also hallmarks of replicative cellular senescence.[59,60] Interestingly, spontaneous decidualization of endometrial stromal cells not only follows intense proliferation prior to ovulation but starts with an acute cellular stress response, characterized by a burst of reactive oxygen species (ROS) production and release of inflammatory mediators.[7,61,62] Further, decidual cells share multiple characteristics with canonical senescent cells, including cell-cycle arrest, expression of survival genes, heightened autonomy from environmental cues, and rounded appearance with abundant cytoplasm and enlarged nuclei.[6] A crucial difference, however, is the suppression of a pro-inflammatory senescence-associated secretory phenotype (SASP) in decidual cells, likely reflecting progesterone-dependent silencing of key pro-inflammatory pathways, including MAPK/JNK,[63] NF-κB,[64] and type 1 interferon signaling.[65,66] Thus, rather than being a novel cell type that originated in ancestral eutherians, as proposed by others,[54,67] decidual cells may represent endometrial stromal cells in which progesterone exerts control over the senescence phenotype and firmly suppresses SASP activation. In keeping with this conjecture, falling progesterone levels prior to menstruation trigger a rapid phenotypic switch in decidual cells, characterized by a rise in $P16^{INK4a}$-positive cells, secretion of extracellular matrix proteinases, inflammatory mediators, and chemokines, and recruitment of macrophages and neutrophils, which in turn reinforce cellular senescence through ROS production.[1] Whether retrotransposition occurs at higher frequency in the endometrium than in other somatic tissues warrants further exploration. However, it is notable that intrinsic mechanisms operate in the endometrium that *a priori* mitigate against the deleterious impacts of transposon activity, including an abundance of uNK cells involved in immune surveillance and clearance of stressed and damaged stromal cells and the wholesale disposal of the decidualizing endometrium at menstruation or following parturition.[1]

Limitations of the study

Although we carefully timed the endometrial biopsies for scATAC-seq analysis, the sample size was limited and insufficient to

assess physiological variability or to detect subtle temporal changes in chromatin accessibility in less abundant cellular constituents, such as ciliated epithelial cells. Furthermore, the coverage of the proliferative phase was sparse in our sample set and requires further validation studies. The biopsies, which contain only superficial endometrium, also did not cover the menstrual phase of the cycle. Further studies are needed to map the changes in DNA methylation and histone modifications associated with dynamic chromatin remodeling and to parse the underlying regulatory mechanisms. Labeling of *de novo* motifs was based on best matches to the HOMER motif database.[23] Motifs were then subjected to validation with the Tomtom Motif Comparison Tool.[68] Some, but not all, motifs were found to match the predicted TF families following FDR correction, which highlights the need for additional ChIP-seq validation studies. Validated motifs are annotated in the corresponding figures. We were only able to infer the impacts of enriched binding motifs in opening and closing scATAC-seq peaks on TF activity and gene expression. Additional genomic investigations, including mapping of cell-type-specific enhancers, are needed to gain granular insights into how cell-specific chromatin changes control the spatiotemporal gene expression in the endometrium. Our observation of widespread TE de-repression and transcription represents an as yet poorly explored dimension in endometrial physiology. The impact of this phenomenon on reproductive health and disease warrants further investigations.

In conclusion, by mapping chromatin accessibility at the single-cell level, we demonstrated that cyclical endometrial remodeling involves highly coordinated changes in chromatin accessibility in endometrial cells, which converge during the implantation window. In stromal cells, this convergence constitutes an inflection point, away from sequential enrichment of specific DNA binding motifs and expression of corresponding TFs and toward cooption of TE-derived complex response elements evolved to assume control over decidual gene expression. Our data constitute a resource for the exploration of gene regulation in cycling human endometrium and the benchmarking of mechanistic studies *in vitro*.

STAR★METHODS

Detailed methods are provided in the online version of this paper and include the following:

- KEY RESOURCES TABLE
- RESOURCE AVAILABILITY
  - Lead contact
  - Materials availability
  - Data and code availability
- EXPERIMENTAL MODEL AND STUDY PARTICIPANT DETAILS
- METHOD DETAILS
  - Timing validation of secretory phase endometrial samples by RT-qPCR
  - Construction and sequencing of scATAC-seq libraries
  - Processing of scATAC-seq data
  - Gene expression inference and analysis of publicly available transcriptomic datasets
  - Temporal analysis of scATAC-seq peaks and similarity scores
  - TF binding motif analyses
  - Transposable elements
  - HNF1B immunohistochemistry
- QUANTIFICATION AND STATISTICAL ANALYSIS
  - Analysis of scATAC-seq peaks
  - Analysis of DNA binding motifs
  - Analysis of transcriptomic datasets

SUPPLEMENTAL INFORMATION

Supplemental information can be found online at https://doi.org/10.1016/j.celrep.2023.113525.

ACKNOWLEDGMENTS

We wish to thank patients attending the Implantation Research Clinic at University Hospitals Coventry and Warwickshire (UHCW) National Health Service Trust (NHS) for contributing endometrial samples for research. We also thank University of Birmingham and University of Warwick Genomics facilities and the staff of the Biomedical Research Unit at UHCW NHS Trust. We are indebted to Dr Katherine Fishwick for assistance with immunohistochemistry. This work was supported by funds from the Tommy's National Miscarriage Research Centre and a joint Wellcome Trust Investigator Award to J.J.B. and S.O. (212233/Z/18/Z). For the purpose of open access, the authors have applied a Creative Commons Attribution (CC-BY) license to any author-accepted manuscript version arising from this submission.

AUTHOR CONTRIBUTIONS

Conceptualization: J.J.B. and S.O.; software: P.V.; methodology: P.V. and E.S.L.; formal analysis: P.V. and J.J.B.; investigation: P.V., J.J.B., E.S.L., J.M., and M.T.; resources: J.J.B.; data curation: P.V., J.J.B., E.S.L., and J.M.; writing – original draft: J.J.B. and P.V.; writing – review and editing: J.J.B., P.V., E.S.L., and J.M.; visualization: P.V., E.S.L., and J.M. supervision: J.J.B. and S.O. funding acquisition: J.J.B. and S.O.

DECLARATION OF INTERESTS

The authors declare no competing interests.

Received: June 7, 2023
Revised: September 21, 2023
Accepted: November 15, 2023
Published: December 5, 2023

REFERENCES

1. Muter, J., Lynch, V.J., McCoy, R.C., and Brosens, J.J. (2023). Human embryo implantation. Development *150*, dev201507.
2. Ferenczy, A., Bertrand, G., and Gelfand, M.M. (1979). Proliferation kinetics of human endometrium during the normal menstrual cycle. Am. J. Obstet. Gynecol. *133*, 859–867.
3. Raine-Fenning, N.J., Campbell, B.K., Clewes, J.S., Kendall, N.R., and Johnson, I.R. (2004). Defining endometrial growth during the menstrual cycle with three-dimensional ultrasound. Bjog *111*, 944–949.
4. Wang, W., Vilella, F., Alama, P., Moreno, I., Mignardi, M., Isakova, A., Pan, W., Simon, C., and Quake, S.R. (2020). Single-cell transcriptomic atlas of the human endometrium during the menstrual cycle. Nat. Med. *26*, 1644–1653.
5. Noyes, R.W., Hertig, A.T., and Rock, J. (2019). Reprint of: Dating the Endometrial Biopsy. Fertil. Steril. *112*, e93–e115.

6. Gellersen, B., and Brosens, J.J. (2014). Cyclic decidualization of the human endometrium in reproductive health and failure. Endocr. Rev. *35*, 851–905.

7. Lucas, E.S., Vrljicak, P., Muter, J., Diniz-da-Costa, M.M., Brighton, P.J., Kong, C.S., Lipecki, J., Fishwick, K.J., Odendaal, J., Ewington, L.J., et al. (2020). Recurrent pregnancy loss is associated with a pro-senescent decidual response during the peri-implantation window. Commun. Biol. *3*, 37.

8. Brighton, P.J., Maruyama, Y., Fishwick, K., Vrljicak, P., Tewary, S., Fujihara, R., Muter, J., Lucas, E.S., Yamada, T., Woods, L., et al. (2017). Clearance of senescent decidual cells by uterine natural killer cells in cycling human endometrium. Elife *6*, e31274.

9. Kong, C.S., Ordoñez, A.A., Turner, S., Tremaine, T., Muter, J., Lucas, E.S., Salisbury, E., Vassena, R., Tiscornia, G., Fouladi-Nashta, A.A., et al. (2021). Embryo biosensing by uterine natural killer cells determines endometrial fate decisions at implantation. Faseb j *35*, e21336.

10. Moffett, A., and Shreeve, N. (2023). Local immune recognition of trophoblast in early human pregnancy: controversies and questions. Nat. Rev. Immunol. *23*, 222–235.

11. Vento-Tormo, R., Efremova, M., Botting, R.A., Turco, M.Y., Vento-Tormo, M., Meyer, K.B., Park, J.E., Stephenson, E., Polański, K., Goncalves, A., et al. (2018). Single-cell reconstruction of the early maternal-fetal interface in humans. Nature *563*, 347–353.

12. DeMayo, F.J., and Lydon, J.P. (2020). 90 YEARS OF PROGESTERONE: New insights into progesterone receptor signaling in the endometrium required for embryo implantation. J. Mol. Endocrinol. *65*. T1-t14.

13. Ruiz-Alonso, M., Blesa, D., Díaz-Gimeno, P., Gómez, E., Fernández-Sánchez, M., Carranza, F., Carrera, J., Vilella, F., Pellicer, A., and Simón, C. (2013). The endometrial receptivity array for diagnosis and personalized embryo transfer as a treatment for patients with repeated implantation failure. Fertil. Steril. *100*, 818–824.

14. Liu, H., Huang, X., Mor, G., and Liao, A. (2020). Epigenetic modifications working in the decidualization and endometrial receptivity. Cell. Mol. Life Sci. *77*, 2091–2101.

15. Osokine, I., Siewiera, J., Rideaux, D., Ma, S., Tsukui, T., and Erlebacher, A. (2022). Gene silencing by EZH2 suppresses TGF-β activity within the decidua to avert pregnancy-adverse wound healing at the maternal-fetal interface. Cell Rep. *38*, 110329.

16. Voss, T.C., and Hager, G.L. (2014). Dynamic regulation of transcriptional states by chromatin and transcription factors. Nat. Rev. Genet. *15*, 69–81.

17. Buenrostro, J.D., Wu, B., Litzenburger, U.M., Ruff, D., Gonzales, M.L., Snyder, M.P., Chang, H.Y., and Greenleaf, W.J. (2015). Single-cell chromatin accessibility reveals principles of regulatory variation. Nature *523*, 486–490.

18. Lipecki, J., Mitchell, A.E., Muter, J., Lucas, E.S., Makwana, K., Fishwick, K., Odendaal, J., Hawkes, A., Vrljicak, P., Brosens, J.J., and Ott, S. (2022). EndoTime: non-categorical timing estimates for luteal endometrium. Hum. Reprod. *37*, 747–761.

19. Cloke, B., Huhtinen, K., Fusi, L., Kajihara, T., Yliheikkilä, M., Ho, K.K., Teklenburg, G., Lavery, S., Jones, M.C., Trew, G., et al. (2008). The androgen and progesterone receptors regulate distinct gene networks and cellular functions in decidualizing endometrium. Endocrinology *149*, 4462–4474.

20. Bennesch, M.A., and Picard, D. (2015). Minireview: Tipping the balance: ligand-independent activation of steroid receptors. Mol. Endocrinol. *29*, 349–363.

21. Giaimo, B.D., Gagliani, E.K., Kovall, R.A., and Borggrefe, T. (2021). Transcription Factor RBPJ as a Molecular Switch in Regulating the Notch Response. Adv. Exp. Med. Biol. *1287*, 9–30.

22. Talbi, S., Hamilton, A.E., Vo, K.C., Tulac, S., Overgaard, M.T., Dosiou, C., Le Shay, N., Nezhat, C.N., Kempson, R., Lessey, B.A., et al. (2006). Molecular phenotyping of human endometrium distinguishes menstrual cycle phases and underlying biological processes in normo-ovulatory women. Endocrinology *147*, 1097–1121.

23. Heinz, S., Benner, C., Spann, N., Bertolino, E., Lin, Y.C., Laslo, P., Cheng, J.X., Murre, C., Singh, H., and Glass, C.K. (2010). Simple combinations of lineage-determining transcription factors prime cis-regulatory elements required for macrophage and B cell identities. Mol. Cell *38*, 576–589.

24. Salker, M.S., Singh, Y., Zeng, N., Chen, H., Zhang, S., Umbach, A.T., Fakhri, H., Kohlhofer, U., Quintanilla-Martinez, L., Durairaj, R.R.P., et al. (2017). Loss of Endometrial Sodium Glucose Cotransporter SGLT1 is Detrimental to Embryo Survival and Fetal Growth in Pregnancy. Sci. Rep. *7*, 12612.

25. Lemeille, S., Paschaki, M., Baas, D., Morlé, L., Duteyrat, J.L., Ait-Lounis, A., Barras, E., Soulavie, F., Jerber, J., Thomas, J., et al. (2020). Interplay of RFX transcription factors 1, 2 and 3 in motile ciliogenesis. Nucleic Acids Res. *48*, 9019–9036.

26. Uhlén, M., Fagerberg, L., Hallström, B.M., Lindskog, C., Oksvold, P., Mardinoglu, A., Sivertsson, Å., Kampf, C., Sjöstedt, E., Asplund, A., et al. (2015). Proteomics. Tissue-based map of the human proteome. Science *347*, 1260419.

27. Moore, L., Leongamornlert, D., Coorens, T.H.H., Sanders, M.A., Ellis, P., Dentro, S.C., Dawson, K.J., Butler, T., Rahbari, R., Mitchell, T.J., et al. (2020). The mutational landscape of normal human endometrial epithelium. Nature *580*, 640–646.

28. Lynch, V.J., Brayer, K., Gellersen, B., and Wagner, G.P. (2009). HoxA-11 and FOXO1A cooperate to regulate decidual prolactin expression: towards inferring the core transcriptional regulators of decidual genes. PLoS One *4*, e6845.

29. Mak, I.Y.H., Brosens, J.J., Christian, M., Hills, F.A., Chamley, L., Regan, L., and White, J.O. (2002). Regulated expression of signal transducer and activator of transcription, Stat5, and its enhancement of PRL expression in human endometrial stromal cells in vitro. J. Clin. Endocrinol. Metab. *87*, 2581–2588.

30. Kuroda, K., Venkatakrishnan, R., Salker, M.S., Lucas, E.S., Shaheen, F., Kuroda, M., Blanks, A., Christian, M., Quenby, S., and Brosens, J.J. (2013). Induction of 11β-HSD 1 and activation of distinct mineralocorticoid receptor- and glucocorticoid receptor-dependent gene networks in decidualizing human endometrial stromal cells. Mol. Endocrinol. *27*, 192–202.

31. Lynch, V.J., Nnamani, M.C., Kapusta, A., Brayer, K., Plaza, S.L., Mazur, E.C., Emera, D., Sheikh, S.Z., Grützner, F., Bauersachs, S., et al. (2015). Ancient transposable elements transformed the uterine regulatory landscape and transcriptome during the evolution of mammalian pregnancy. Cell Rep. *10*, 551–561.

32. Lynch, V.J., Leclerc, R.D., May, G., and Wagner, G.P. (2011). Transposon-mediated rewiring of gene regulatory networks contributed to the evolution of pregnancy in mammals. Nat. Genet. *43*, 1154–1159.

33. Mika, K., and Lynch, V.J. (2022). Transposable Elements Continuously Remodel the Regulatory Landscape, Transcriptome, and Function of Decidual Stromal Cells. Genome Biol. Evol. *14*, evac164.

34. Shen, M.R., Batzer, M.A., and Deininger, P.L. (1991). Evolution of the master Alu gene(s). J. Mol. Evol. *33*, 311–320.

35. Mika, K.M., Li, X., DeMayo, F.J., and Lynch, V.J. (2018). An Ancient Fecundability-Associated Polymorphism Creates a GATA2 Binding Site in a Distal Enhancer of HLA-F. Am. J. Hum. Genet. *103*, 509–521.

36. Vasquez, Y.M., Mazur, E.C., Li, X., Kommagani, R., Jiang, L., Chen, R., Lanz, R.B., Kovanci, E., Gibbons, W.E., and DeMayo, F.J. (2015). FOXO1 is required for binding of PR on IRF4, novel transcriptional regulator of endometrial stromal decidualization. Mol. Endocrinol. *29*, 421–433.

37. Mazur, E.C., Vasquez, Y.M., Li, X., Kommagani, R., Jiang, L., Chen, R., Lanz, R.B., Kovanci, E., Gibbons, W.E., and DeMayo, F.J. (2015). Progesterone receptor transcriptome and cistrome in decidualized human endometrial stromal cells. Endocrinology *156*, 2239–2253.

38. Hawkins Bressler, L., Fritz, M.A., Wu, S.P., Yuan, L., Kafer, S., Wang, T., DeMayo, F.J., and Young, S.L. (2021). Poor Endometrial Proliferation After

Clomiphene is Associated With Altered Estrogen Action. J. Clin. Endocrinol. Metab. *106*, 2547–2565.

39. Gertz, J., Savic, D., Varley, K.E., Partridge, E.C., Safi, A., Jain, P., Cooper, G.M., Reddy, T.E., Crawford, G.E., and Myers, R.M. (2013). Distinct properties of cell-type-specific and shared transcription factor binding sites. Mol. Cell *52*, 25–36.
40. Rubel, C.A., Wu, S.P., Lin, L., Wang, T., Lanz, R.B., Li, X., Kommagani, R., Franco, H.L., Camper, S.A., Tong, Q., et al. (2016). A Gata2-Dependent Transcription Network Regulates Uterine Progesterone Responsiveness and Endometrial Function. Cell Rep. *17*, 1414–1425.
41. Garcia-Alonso, L., Handfield, L.F., Roberts, K., Nikolakopoulou, K., Fernando, R.C., Gardner, L., Woodhams, B., Arutyunyan, A., Polanski, K., Hoo, R., et al. (2021). Mapping the temporal and spatial dynamics of the human endometrium in vivo and in vitro. Nat. Genet. *53*, 1698–1711.
42. Rodríguez-Quiroz, R., and Valdebenito-Maturana, B. (2022). SoloTE for improved analysis of transposable elements in single-cell RNA-Seq data using locus-specific expression. Commun. Biol. *5*, 1063.
43. Boissinot, S., Entezam, A., Young, L., Munson, P.J., and Furano, A.V. (2004). The insertional history of an active family of L1 retrotransposons in humans. Genome Res. *14*, 1221–1231.
44. Burns, K.H. (2017). Transposable elements in cancer. Nat. Rev. Cancer *17*, 415–424.
45. Gargett, C.E., and Rogers, P.A. (2001). Human endometrial angiogenesis. Reproduction *121*, 181–186.
46. Iruela-Arispe, M.L., Rodriguez-Manzaneque, J.C., and Abu-Jawdeh, G. (1999). Endometrial endothelial cells express estrogen and progesterone receptors and exhibit a tissue specific response to angiogenic growth factors. Microcirculation *6*, 127–140.
47. Strunz, B., Bister, J., Jönsson, H., Filipovic, I., Crona-Guterstam, Y., Kvedaraite, E., Sleiers, N., Dumitrescu, B., Brännström, M., Lentini, A., et al. (2021). Continuous human uterine NK cell differentiation in response to endometrial regeneration and pregnancy. Sci. Immunol. *6*, eabb7800.
48. Rytkönen, K.T., Erkenbrack, E.M., Poutanen, M., Elo, L.L., Pavlicev, M., and Wagner, G.P. (2019). Decidualization of Human Endometrial Stromal Fibroblasts is a Multiphasic Process Involving Distinct Transcriptional Programs. Reprod. Sci. *26*, 323–336.
49. Ashary, N., Laheri, S., and Modi, D. (2020). Homeobox genes in endometrium: from development to decidualization. Int. J. Dev. Biol. *64*, 227–237.
50. Senft, A.D., and Macfarlan, T.S. (2021). Transposable elements shape the evolution of mammalian development. Nat. Rev. Genet. *22*, 691–711.
51. Mika, K., Marinić, M., Singh, M., Muter, J., Brosens, J.J., and Lynch, V.J. (2021). Evolutionary transcriptomics implicates new genes and pathways in human pregnancy and adverse pregnancy outcomes. Elife *10*, e69584.
52. Chavan, A.R., Bhullar, B.A.S., and Wagner, G.P. (2016). What was the ancestral function of decidual stromal cells? A model for the evolution of eutherian pregnancy. Placenta *40*, 40–51.
53. Vrljicak, P., Lucas, E.S., Lansdowne, L., Lucciola, R., Muter, J., Dyer, N.P., Brosens, J.J., and Ott, S. (2018). Analysis of chromatin accessibility in decidualizing human endometrial stromal cells. Faseb j *32*, 2467–2477.
54. Erkenbrack, E.M., Maziarz, J.D., Griffith, O.W., Liang, C., Chavan, A.R., Nnamani, M.C., and Wagner, G.P. (2018). The mammalian decidual cell evolved from a cellular stress response. PLoS Biol. *16*, e2005594.
55. Christian, M., Zhang, X., Schneider-Merck, T., Unterman, T.G., Gellersen, B., White, J.O., and Brosens, J.J. (2002). Cyclic AMP-induced forkhead transcription factor, FKHR, cooperates with CCAAT/enhancer-binding protein beta in differentiating human endometrial stromal cells. J. Biol. Chem. *277*, 20825–20832.
56. Christian, M., Pohnke, Y., Kempf, R., Gellersen, B., and Brosens, J.J. (2002). Functional association of PR and CCAAT/enhancer-binding protein beta isoforms: promoter-dependent cooperation between PR-B and liver-enriched inhibitory protein, or liver-enriched activatory protein and PR-A in human endometrial stromal cells. Mol. Endocrinol. *16*, 141–154.
57. Chuong, E.B., Elde, N.C., and Feschotte, C. (2017). Regulatory activities of transposable elements: from conflicts to benefits. Nat. Rev. Genet. *18*, 71–86.
58. Gorbunova, V., Seluanov, A., Mita, P., McKerrow, W., Fenyö, D., Boeke, J.D., Linker, S.B., Gage, F.H., Kreiling, J.A., Petrashen, A.P., et al. (2021). The role of retrotransposable elements in ageing and age-associated diseases. Nature *596*, 43–53.
59. De Cecco, M., Criscione, S.W., Peckham, E.J., Hillenmeyer, S., Hamm, E.A., Manivannan, J., Peterson, A.L., Kreiling, J.A., Neretti, N., and Sedivy, J.M. (2013). Genomes of replicatively senescent cells undergo global epigenetic changes leading to gene silencing and activation of transposable elements. Aging Cell *12*, 247–256.
60. Zhang, X., Jiang, Q., Li, J., Zhang, S., Cao, Y., Xia, X., Cai, D., Tan, J., Chen, J., and Han, J.D.J. (2022). KCNQ1OT1 promotes genome-wide transposon repression by guiding RNA-DNA triplexes and HP1 binding. Nat. Cell Biol. *24*, 1617–1629.
61. Al-Sabbagh, M., Fusi, L., Higham, J., Lee, Y., Lei, K., Hanyaloglu, A.C., Lam, E.W.F., Christian, M., and Brosens, J.J. (2011). NADPH oxidase-derived reactive oxygen species mediate decidualization of human endometrial stromal cells in response to cyclic AMP signaling. Endocrinology *152*, 730–740.
62. Salker, M.S., Nautiyal, J., Steel, J.H., Webster, Z., Sućurović, S., Nicou, M., Singh, Y., Lucas, E.S., Murakami, K., Chan, Y.W., et al. (2012). Disordered IL-33/ST2 activation in decidualizing stromal cells prolongs uterine receptivity in women with recurrent pregnancy loss. PLoS One *7*, e52252.
63. Leitao, B., Jones, M.C., Fusi, L., Higham, J., Lee, Y., Takano, M., Goto, T., Christian, M., Lam, E.W.F., and Brosens, J.J. (2010). Silencing of the JNK pathway maintains progesterone receptor activity in decidualizing human endometrial stromal cells exposed to oxidative stress signals. Faseb j *24*, 1541–1551.
64. Kalkhoven, E., Wissink, S., van der Saag, P.T., and van der Burg, B. (1996). Negative interaction between the RelA(p65) subunit of NF-kappaB and the progesterone receptor. J. Biol. Chem. *271*, 6217–6224.
65. Walter, K.R., Goodman, M.L., Singhal, H., Hall, J.A., Li, T., Holloran, S.M., Trinca, G.M., Gibson, K.A., Jin, V.X., Greene, G.L., and Hagan, C.R. (2017). Interferon-Stimulated Genes Are Transcriptionally Repressed by PR in Breast Cancer. Mol. Cancer Res. *15*, 1331–1340.
66. Hughes, G.C., and Choubey, D. (2014). Modulation of autoimmune rheumatic diseases by oestrogen and progesterone. Nat. Rev. Rheumatol. *10*, 740–751.
67. Wagner, G.P., Erkenbrack, E.M., and Love, A.C. (2019). Stress-Induced Evolutionary Innovation: A Mechanism for the Origin of Cell Types. Bioessays *41*, e1800188.
68. Gupta, S., Stamatoyannopoulos, J.A., Bailey, T.L., and Noble, W.S. (2007). Quantifying similarity between motifs. Genome Biol. *8*, R24.
69. Satpathy, A.T., Granja, J.M., Yost, K.E., Qi, Y., Meschi, F., McDermott, G.P., Olsen, B.N., Mumbach, M.R., Pierce, S.E., Corces, M.R., et al. (2019). Massively parallel single-cell chromatin landscapes of human immune cell development and intratumoral T cell exhaustion. Nat. Biotechnol. *37*, 925–936.
70. Stuart, T., Srivastava, A., Madad, S., Lareau, C.A., and Satija, R. (2021). Single-cell chromatin state analysis with Signac. Nat. Methods *18*, 1333–1341.
71. Castro-Mondragon, J.A., Riudavets-Puig, R., Rauluseviciute, I., Lemma, R.B., Turchi, L., Blanc-Mathieu, R., Lucas, J., Boddie, P., Khan, A., Manosalva Pérez, N., et al. (2022). JASPAR 2022: the 9th release of the open-access database of transcription factor binding profiles. Nucleic Acids Res. *50*. D165-d173.
72. Zheng, G.X.Y., Terry, J.M., Belgrader, P., Ryvkin, P., Bent, Z.W., Wilson, R., Ziraldo, S.B., Wheeler, T.D., McDermott, G.P., Zhu, J., et al. (2017). Massively parallel digital transcriptional profiling of single cells. Nat. Commun. *8*, 14049.

73. Love, M.I., Huber, W., and Anders, S. (2014). Moderated estimation of fold change and dispersion for RNA-seq data with DESeq2. Genome Biol. *15*, 550.

74. Dobin, A., Davis, C.A., Schlesinger, F., Drenkow, J., Zaleski, C., Jha, S., Batut, P., Chaisson, M., and Gingeras, T.R. (2013). STAR: ultrafast universal RNA-seq aligner. Bioinformatics *29*, 15–21.

75. Jin, Y., Tam, O.H., Paniagua, E., and Hammell, M. (2015). TEtranscripts: a package for including transposable elements in differential expression analysis of RNA-seq datasets. Bioinformatics *31*, 3593–3599.

76. Thomas, P.D., Ebert, D., Muruganujan, A., Mushayahama, T., Albou, L.P., and Mi, H. (2022). PANTHER: Making genome-scale phylogenetics accessible to all. Protein Sci. *31*, 8–22.

77. Zhang, Y., Liu, T., Meyer, C.A., Eeckhoute, J., Johnson, D.S., Bernstein, B.E., Nusbaum, C., Myers, R.M., Brown, M., Li, W., and Liu, X.S. (2008). Model-based analysis of ChIP-Seq (MACS). Genome Biol. *9*, R137.

78. Stuart, T., Butler, A., Hoffman, P., Hafemeister, C., Papalexi, E., Mauck, W.M., 3rd, Hao, Y., Stoeckius, M., Smibert, P., and Satija, R. (2019). Comprehensive Integration of Single-Cell Data. Cell *177*, 1888–1902.e21.

79. Hu, H., Miao, Y.R., Jia, L.H., Yu, Q.Y., Zhang, Q., and Guo, A.Y. (2019). AnimalTFDB 3.0: a comprehensive resource for annotation and prediction of animal transcription factors. Nucleic Acids Res. *47*. D33-d38.

STAR★METHODS

KEY RESOURCES TABLE

REAGENT or RESOURCE	SOURCE	IDENTIFIER
Antibodies		
Anti-HNF1B	Sigma-Aldrich	HPA002083; RRID: AB_1080232
Oligonucleotides		
Primer: GPX3 Forward: GGGACAAGAGAAGTCGAAGA	This paper	N/A
Primer: GPX3 Reverse: GCCAGCATACTGCTTGAAGG	This paper	N/A
Primer: SLC15A2 Forward: AGGAGGCATCAAACCCTGT	This paper	N/A
Primer: SLC15A2 Reverse: CTAGTCCGTTCCTCTGCATG	This paper	N/A
Deposited data		
Raw and analyzed single-cell ATAC sequencing data	This paper	GEO: GSE183771
Raw and analyzed single-cell RNA sequencing data	Lucas et al.[7]	GEO: GSE127918
Raw single-cell RNA sequencing data	Wang et al.[4]	GEO: GSE111976
Raw single-cell RNA sequencing data	Vento-Tormo et al.[11]	ArrayExpress: PRJEB28266
Raw RNA sequencing data	Salker et al.[24]	GEO: GSE84169
Microarray data	Talbi et al.[22]	GEO: GSE4888
Spatial transcriptomics data	Garcia-Alonso et al.[41]	ArrayExpress: E-MTAB-9260; 152807
GATA2; HECs	Mika et al.[35]	GEO: GSM2897813
FOXO1; HECs	Vasquez et al.[36]	GEO: GSM1703607
FOSL2; HECs	Mazur et al.[37]	GEO: GSM1703568
ESR; late proliferative endometrial biopsy	Hawkins et al.[38]	GEO: GSM5018484
ESR7; late proliferative endometrial biopsy	Hawkins et al.[38]	GEO: GSM5018485
ESR8; late proliferative endometrial biopsy	Hawkins et al.[38]	GEO: GSM5018486
ESR9; late proliferative endometrial biopsy	Hawkins et al.[38]	GEO: GSM5018487
CEBPB; MCF7	Gertz et al.[39]	GEO: GSM1010889
CEBPB; K562	Gertz et al.[39]	GEO: GSM1010878
CEBPB; K549	Gertz et al.[39]	GEO: GSM1010871
CEBPB; HepG2	Gertz et al.[39]	GEO: GSM1010778
CEBPB; GM12878	Gertz et al.[39]	GEO: GSM1010850
Control; HECs – FOXO1	Vasquez et al.[36]	GEO: GSM1703609
Control; HECs – FOSL2	Mazur et al.[37]	GEO: GSM1703569
Control; HECs – GATA2	Mika et al.[35]	GEO: GSM2897814
Control; late proliferative endometrial biopsy - ESR	Hawkins et al.[38]	GEO: GSM5018488
Control; MCF7	Gertz et al.[39]	GEO: GSM1010854
Control; K562	Gertz et al.[39]	GEO: GSM1010894
Control; K549	Gertz et al.[39]	GEO: GSM1010866
Control; HepG2	Gertz et al.[39]	GEO: GSM803521
Control; GM12878	Gertz et al.[39]	GEO: GSM1010867
Software and algorithms		
Cell Ranger	Zheng et al.[69]	https://support.10xgenomics.com/single-cell-gene-expression/software/overview/welcome
DESeq2	Love et al.[70]	https://doi.org/10.18129/B9.bioc.DESeq2
ggplot2	Hadley Wickham	https://ggplot2.tidyverse.org/

(*Continued on next page*)

Continued

REAGENT or RESOURCE	SOURCE	IDENTIFIER
gplots	Tal Galili	https://github.com/talgalili/gplots
HOMER	Heinz et al.[23]	http://homer.ucsd.edu/homer/
ImageJ	National Institutes of Health	https://imagej.nih.gov/ij/
JASPAR	Castro-Mondragon et al.[71]	http://jaspar.genereg.net/
MACS2	Zhang et al.[72]	https://pypi.org/project/MACS2/
PANTHER	Thomas et al.[73]	http://pantherdb.org/
Seurat	Satija Lab	https://satijalab.org/seurat/
Signac	Stuart Lab	https://stuartlab.org/signac/
SoloTE	Rodriguez-Quiroz et al.[42]	https://github.com/bvaldebenitom/SoloTE/
STAR	Dobin et al.[74]	https://github.com/alexdobin/STAR
TEtranscripts	Jin et al.[75]	https://github.com/mhammell-laboratory/TEtranscripts
Tomtom	Gupta et al.[76]	https://meme-suite.org/meme/doc/tomtom.html

RESOURCE AVAILABILITY

Lead contact

Further information and requests for resources and reagents should be directed to and will be fulfilled by the lead contact, Jan Brosens (J.J.Brosens@warwick.ac.uk).

Materials availability

This study did not generate new reagents.

Data and code availability

- The scATAC-seq data have been deposited at GEO and are publicly available. Accession numbers are listed in the key resources table. This paper analyses publicly available data sets. The accession numbers for the datasets are listed in the key resources table. Immunohistochemistry data reported in this study will be shared by the lead contact upon request.
- This paper does not report original code.
- Any additional information required to reanalyze the data reported in this study is available from the lead contact upon request.

EXPERIMENTAL MODEL AND STUDY PARTICIPANT DETAILS

The study was approved by the National Health Service (NHS) National Research Ethics-Hammersmith and Queen Charlotte's and Chelsea Research Ethics Committee (REC ref. 1997/5065) and Tommy's National Reproductive Health Biobank (REC ref. 18/WA/0356). Endometrial biopsies, timed relative to the last menstrual period or patient-reported pre-ovulatory luteinizing hormone (LH) surge following ovulation testing, were collected at the Implantation Research Clinic, a dedicated research clinic at University Hospitals Coventry and Warwickshire (UHCW) NHS Trust. Endometrial samples were obtained using a Wallach Endocell sampler (Wallach Surgical Devices, Trumbull, USA) and snap frozen immediately in LN2 before storage at −80°C. Written informed consent was obtained from all participants in accordance with The Declaration of Helsinki 2000 guidelines. Anonymized endometrial biopsies were obtained from women aged between 32 and 41 years with regular cycles, body mass index between 19 and 30 kg/m^2, and absence of overt uterine pathology on transvaginal ultrasound examination. Demographic details of the tissue samples are shown in Table S1.

METHOD DETAILS

Timing validation of secretory phase endometrial samples by RT-qPCR

Timing of secretory phase biopsies was validated by calculating the ratio of *GPX3* and *SLC15A2* gene expression as measured by RT-qPCR. RNA was extracted from endometrial biopsies which had been snap frozen in clinic (<1 min after collection), using STAT-60 (AMS Biotechnology, Oxford, UK) according to the manufacturer's instructions. Reverse transcription was performed from 1 μg RNA using the Quantitect Reverse Transcription Kit (QIAGEN, Manchester, UK) and cDNA was diluted to 10 ng/μL equivalent before use in qPCR. Amplification was performed on a 7500 Real-Time PCR system (Applied Biosystems, Paisley, UK) in 20 μL reactions using 2 × PrecisionPlus Mastermix with SYBR Green and low ROX (PrimerDesign, Southampton, UK), with 300 nM each of forward and reverse primers. Primer sequences were as follows: *GPX3* forward: 5′-GGG GAC AAG AGA AGT CGA AGA-3′, *GPX3* reverse:

5′-GCC AGC ATA CTG CTT GAA GG-3'; *SLC15A2* forward: 5′- AGG AGG CAT CAA ACC CTG T-3′, *SLC15A2* reverse: 5′- CTA GTC CGT TCC TCT GCA TG-3'.

Construction and sequencing of scATAC-seq libraries

Twelve timed endometrial biopsies, processed as described in detail elsewhere,[8] were subjected to scATAC-seq. All protocols for nuclei isolation and library construction have been described previously,[69] and available at https://support.10xgenomics.com/single-cell-atac. Briefly, nuclei were extracted according to the 10X Genomics demonstrated protocol for frozen tissue (CG000212 Rev B), modified to include an additional wash with Wash Buffer. Tissue homogenization was performed using a Dounce homogenizer. Filtered nuclei suspension was pelleted as instructed and then resuspended in 50 μl Storage Buffer from the EZ nuclei kit (Sigma Aldrich, NUC101). For downstream processing, nuclei were thawed briefly on ice, resuspended with 500 μl Wash Buffer and gently pipetted. Nuclei were pelleted at 500 × g (5 min, 4°C) then resuspended again in 500 μl Wash Buffer before counting and continuing to Chromium capture. scATAC-seq libraries were generated according to the Chromium Single Cell ATAC protocol (10X GENOMICS, CG000168) as described previously[69] and sequenced on the Illumina NextSeq 500 platform. The sequencing data were deposited in the GEO repository (https://www.ncbi.nlm.nih.gov/geo/) under accession number GSE183771.

Processing of scATAC-seq data

Cell Ranger ATAC pipeline version 1.2.0[72] was used for data pre-processing and alignment to the GRCh38 human genome assembly (refdata-cellranger-atac-GRCh38–1.2.0). When applicable, the number of fragments overlapping peaks was examined to correct the estimated number of nuclei. Peak calling was carried out on a merged BAM file using MACS2,[77] leading to the identification of 403,434 peaks. 276,524 of these peaks were deemed high confidence ($q < 1 \times 10^{-4}$) and were used for further analysis. Analysis of scATAC-seq libraries, including clustering and UMAP projection was carried out with Seurat v3.2.2[78] and Signac v0.2.5[70] R packages. Count data was normalized using the RunTFIDF function with a scale factor of 10000. Dimensionality reduction was performed with the RunSVD function with latent semantic indexing (LSI), following which nuclei clustering and UMAP embedding was carried out with the first 50 components. The Seurat function FindAllMarkers and FindMarkers employing the Wilcoxon test was used to identify differential chromatin opening for each cell-type in the UMAP representation. Differential opening was considered significant if the Bonferroni corrected p value was less than 0.05.

Gene expression inference and analysis of publicly available transcriptomic datasets

Inference of gene expression levels from scATAC-seq data was performed with Signac by summing all counts from 2000 bp upstream of the transcriptional start site to the transcriptional termination site. Analysis of three endometrial scRNA-seq datasets (GEO accession GSE127918 and GSE111976, and ArrayExpress PRJEB28266)[4,7,11] was performed using Seurat v3.2.2.[78] The Seurat AverageExpression function was used to calculate average gene expression of published cell-types and the Seurat function FindMarkers employing the Wilcoxon test was used to identify differential gene expression. Glandular epithelial gene expression was analyzed from published RNA-seq data (GEO accession GSE84169),[24] using the DESeq2 v1.30.1 package in R.[73] Expression profiling by array of human endometrium (GEO accession GSE4888)[22] was visualized with heatmap function of gplots v3.1.3 package in R. Gene Ontology enrichment analysis was performed with PANTHER.[76]

Temporal analysis of scATAC-seq peaks and similarity scores

To perform temporal pattern analysis of chromatin changes in secretory phase samples, scATAC-seq peaks with temporal variation were first selected by pairwise comparisons. Peaks with at least one significant change (Bonferroni corrected $p < 0.05$) between secretory samples were then grouped into temporal patterns by K-means clustering on scaled averaged values. To measure the likelihood of non-clustered peaks fitting the secretory phase temporal patterns, we devised similarity scores. At every timepoint, the average opening of the peak was compared against the mean and standard deviation obtained from all the peaks in a temporal pattern to produce a *Z* score. Finally, an overall similarity score was obtained by adding the absolute value of the individual z-scores and subtracting this value from the maximum such that higher similarity scores represented peaks with a pattern close to the original (Figures S2C and S3C). The similarity score where temporally regulated chromatin regions crossover with all other peaks was used as the minimum cutoff for the selection of expanded temporal sets (Figure S3C).

TF binding motif analyses

Differentially opening chromatin regions were interrogated for enriched short sequence motifs using HOMER v4.8.[23] To establish the significance cutoff for enriched motifs, the analysis was repeated 5 times on shuffled data. Specifically, the pattern identifiers for the temporally regulated loci were randomly shuffled to produce sets of peaks of the same length as the originals but without meaningful temporal correlation. The least significant p value obtained from the 5 analyses on shuffled data was deemed the significant cutoff for the corresponding temporal pattern. Footprint and PlotFootprint functions in Signac were used to visualize the average chromatin opening pattern around the identified motifs. Chromatin opening at a specific site was visualized with the CoveragePlot function in Signac and adapted using the ggplot2 R package. TF family prediction was based on HOMER best match and validated by scanning the HOMER and JASPAR databases with Tomtom.[68] The results are tabulated in Table S1C. To help predict the specific transcription factors responsible for the observed chromatin changes, every TF from the enriched families were first identified using

AnimalTFDB v3,[79] then examined RNA expression of members of TF families identified.[4] For ESR and PGR binding site enrichment analysis, the entire genome was scanned for ERE and PRE motifs in HOMER using the findmotifs function. Peaks were assigned as harboring ERE sites if they overlapped by at least 1bp with the HOMER motif derived from ERα ChIP-seq experiments in MCF7 cells. Peaks were annotated as containing PRE sites if they overlapped by at least 1bp with both PGR motifs in the HOMER database derived from ChIP-seq experiments in human endometrial stromal cells and T47D breast cancer cells, respectively.

Transposable elements

Genomic coordinates for repetitive elements were obtained from the RepeatMasker track of the UCSC genome browser (A.F.A. Smit, R. Hubley & P. Green RepeatMasker at http://repeatmasker.org). Enrichment of repeats overlapping expanded temporal chromatin opening patterns was calculated using the hypergeometric distribution in R. Full length Alu sequences were analyzed for evidence of transposase accessibility. TFBSs predictions for ESR1, FOSL2, GATA2, FOXO1, and CEBPB were obtained from JASPAR track in UCSC browser.[71] TF binding data were obtained from published ChIP-seq datasets.[35–39] Peak summits were generated with MACS2[77] on sequencing files mapped to the hg38 genome assembly using STAR aligner.[74] For spatial mapping of TE-derived transcripts in the endometrium and adjacent myometrium, we reanalyzed publicly available Visium (10X GENOMICS) data (ArrayExpress ID: E-MTAB-9260; 152807).[41] Locus-specific quantification of TE-derived transcripts in the spatial transcriptomic data was performed with SoloTE.[42] The resulting count matrix was used for single-cell analysis using Seurat. Visualization was performed by aggregating the normalized expression of TE families. Quantification of L1 and Alu derived RNA expression in bulk RNA-seq data (GEO accession GSE180485) was performed with TEtranscripts.[75]

HNF1B immunohistochemistry

Endometrial biopsies were fixed overnight in 10% neutral buffered formalin at 4°C and wax embedded in Surgipath Formula 'R' paraffin (Leica BioSystems, Wetzlar, Germany) using the Shandon Excelsior ES Tissue processor (ThermoFisher Scientific, Massachusetts, US). Tissues were sliced into 3 μm sections using a microtome and adhered to coverslips by overnight incubation at 60°C. Deparaffinization, antigen retrieval (sodium citrate buffer; 10 mM sodium citrate, 0.05% Tween 20, pH 6), antibody staining, haematoxylin counter stain and DAB color development were fully automated in a Leica BondMax autostainer (Leica BioSystems, Wetzlar, Germany). Tissue sections were labeled for HNF1B (HPA002083, Prestige Antibodies Powered by Atlas Antibodies, Sigma-Aldrich, Missouri, US) using a 1:1000 dilution. Stained slides were de-hydrated, cleared and cover-slipped in a Tissue-Tek Prisma Automated Slide Stainer, model 6134 (Sakura Flinetek, Inc., California, US) using DPX coverslip mountant. Bright-field images were obtained on a Mirax Midi slide scanner with a 20× objective lens and viewed in CaseViewer v2.4.0.1198028 (3DHISTECH Ltd, Budapest, Hungary). Three randomly selected areas of interest underlying the luminal epithelium were captured and each of the regions was divided manually into three compartments: stroma, glandular epithelium, and luminal epithelium. ImageJ image analysis software (Rasband, W.S., ImageJ, National Institutes of Health) was used to quantify $HNF1B^+$ cells in the glandular epithelium with staining intensity manually determined by background thresholding. The percentage of $HNF1B^+$ cells was calculated (i.e., $HNF1B^+$ cells/total cells ×100) in each region of view for the glandular epithelium.

QUANTIFICATION AND STATISTICAL ANALYSIS

Analysis of scATAC-seq peaks

The Wilcoxon rank-sum test was used to identify differential chromatin peaks between cell types. Bonferroni corrected $p < 0.05$ was considered statistically significant. For temporal clustering of open chromatin regions, K-means clustering was performed on scaled averaged values. The value of K was determined by identifying the elbow point in a plot of within-cluster sum of squares. The trend curve, representing average expression per timepoint, was calculated by applying locally estimated scatterplot smoothing (LOESS) fit ±standard error of mean (SEM).

Analysis of DNA binding motifs

The Chi-squared test was used to examine quantitative differences in the proportion of scATAC-seq peaks overlapping ERE, PRE or both motifs between stromal cells (SC) or epithelial cells (EpC) in proliferative versus secretory endometrial samples. Figure 2A shows p values for specific comparisons. Differentially accessible chromatin regions were interrogated for short sequence motif enrichment using HOMER.[23] Zero or one occurrence per sequence scoring (ZOOPS) coupled to hypergeometric enrichment calculations was used to determine motif enrichment. Closest known motif matches were evaluated with Tomtom,[68] with p values representing the probability of a random motif of the same width having an alignment score as good or better than the target. The *q* values in Table S1C are based on the Benjamini and Hochberg method. The hypergeometric test was used to interrogate the proportion of TEs overlapping temporally regulated chromatin regions.

Analysis of transcriptomic datasets

Publicly available gene expression datasets, tabulated in Table S1B, were interrogated as described in the method details. The Wilcoxon rank-sum test was used to identify differentially expressed genes with Bonferroni corrected $p < 0.05$ considered significant.

Gene Ontology enrichment analysis performed with PANTHER[76] uses the Wilcoxon rank-sum test. Spatial transcriptomics analysis was performed on a hysterectomy specimen obtained in the early secretory phase of the menstrual cycle as described in method details. Counts of locus specific TE elements were summed per spot to obtain overall counts per TE family. The Wilcoxon rank-sum test followed by Bonferroni correction was used to determine differentially expressed TE transcripts in one region against all other regions as shown in Figure 5D. Normalized average expression of TE-derived transcripts across the four regions was used to calculate the change in relative expression from the mean.

Cell Reports, Volume *42*

Supplemental information

Dynamic chromatin remodeling in cycling human endometrium at single-cell level

Pavle Vrljicak, Emma S. Lucas, Maria Tryfonos, Joanne Muter, Sascha Ott, and Jan J. Brosens

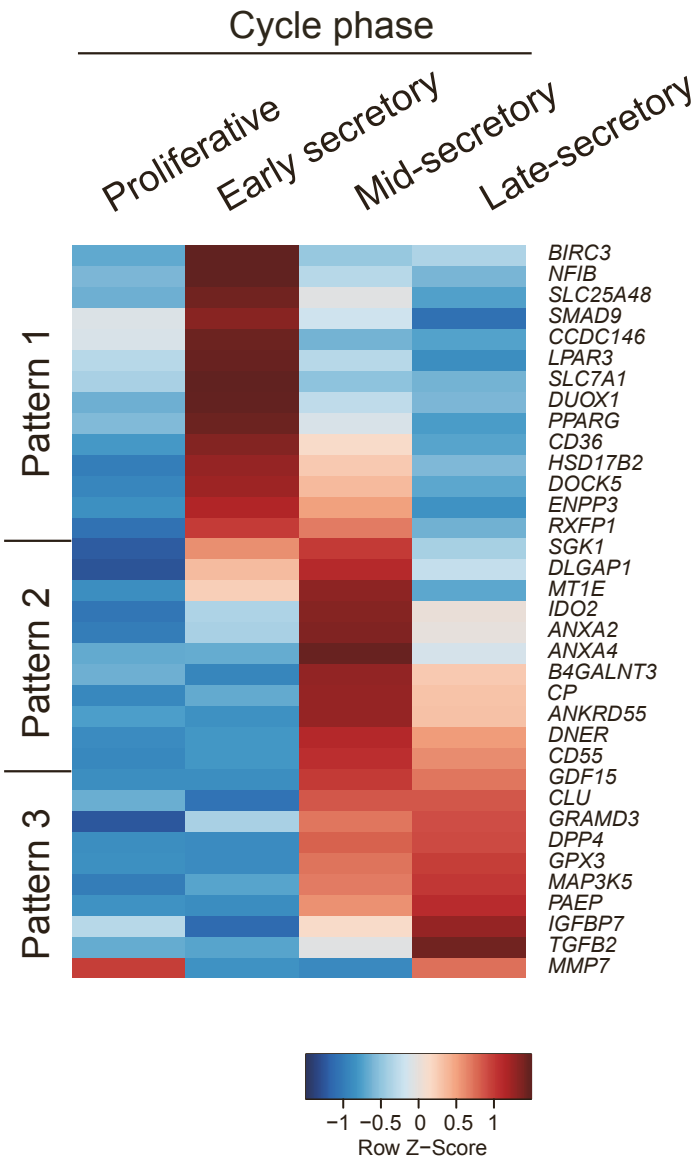

Figure S1, related to Figure 3. Heatmap of epithelial cell-enriched genes nearest to temporally regulated accessible chromatin loci in whole tissue expression data across the menstrual cycle. [S1]

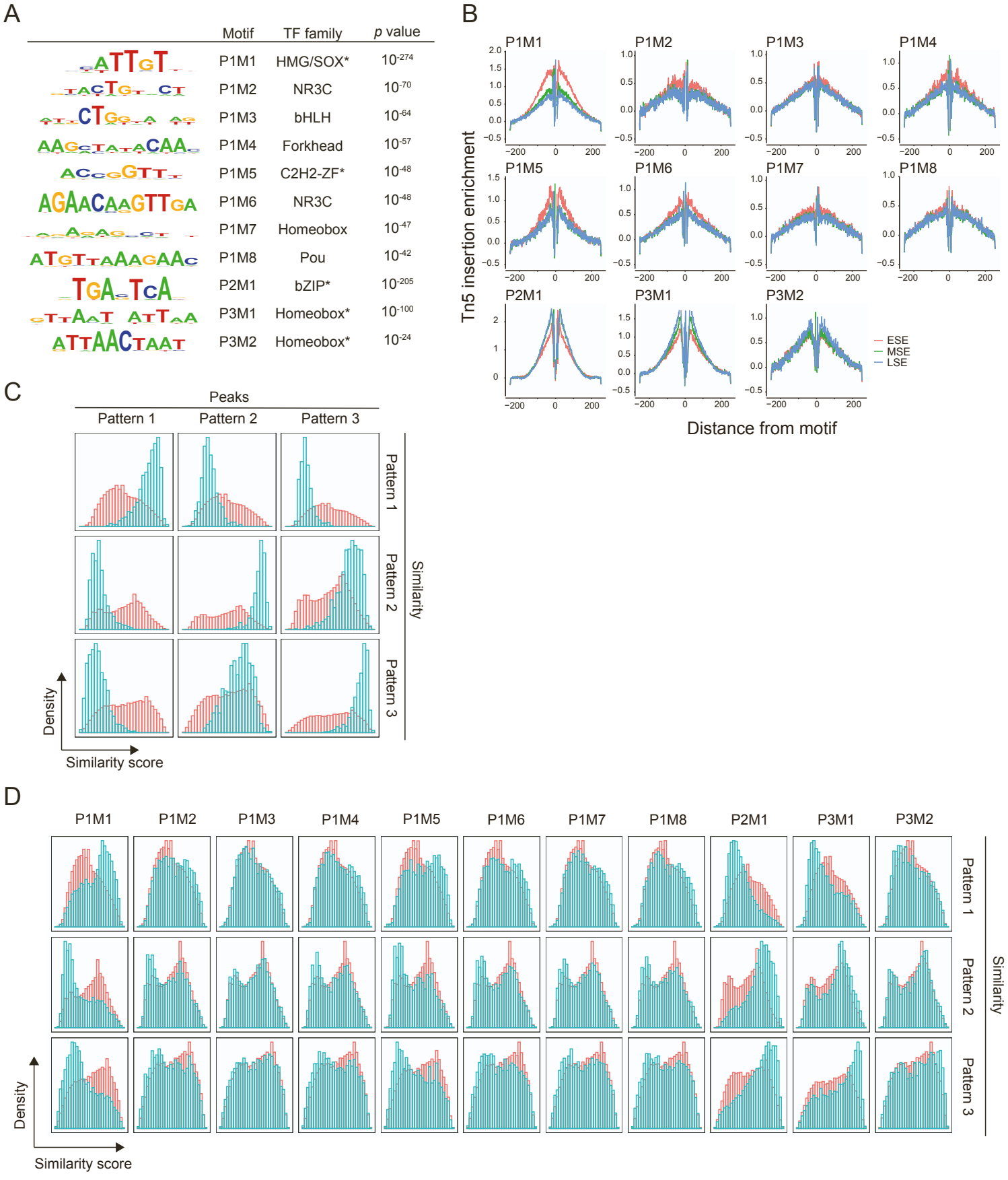

Figure S2, related to Figure 3. Enriched TF binding motifs in temporally regulated chromatin regions in differentiating epithelial cells.

(A) Table of enriched motifs. *P* values represent binomial test results using HOMER [S2]. Motifs shown are significantly enriched based on *p* value threshold determined by performing analysis 5 times on shuffled chromatin regions. Best TF family matches were based on known motifs in the HOMER motif database (Table S1C). * indicates statistically significant TF family matches (FDR corrected *p* value < 0.05).

(B) Footprint analysis of temporally enriched motifs from panel A. Average transposase insertion centered around the motifs. Secretory samples were grouped as early-secretory endometrium (ESE; S18-19), mid-secretory endometrium (MSE; S20-21) or late-secretory endometrium (LSE; S22-25).

(C) All ATAC-seq peaks in differentiating epithelial cells scored according to their temporal pattern similarity. Validation of pattern enrichment score in differentiating epithelial cells.

(D) ATAC-seq peaks grouped by presence of enriched motifs from panel A.

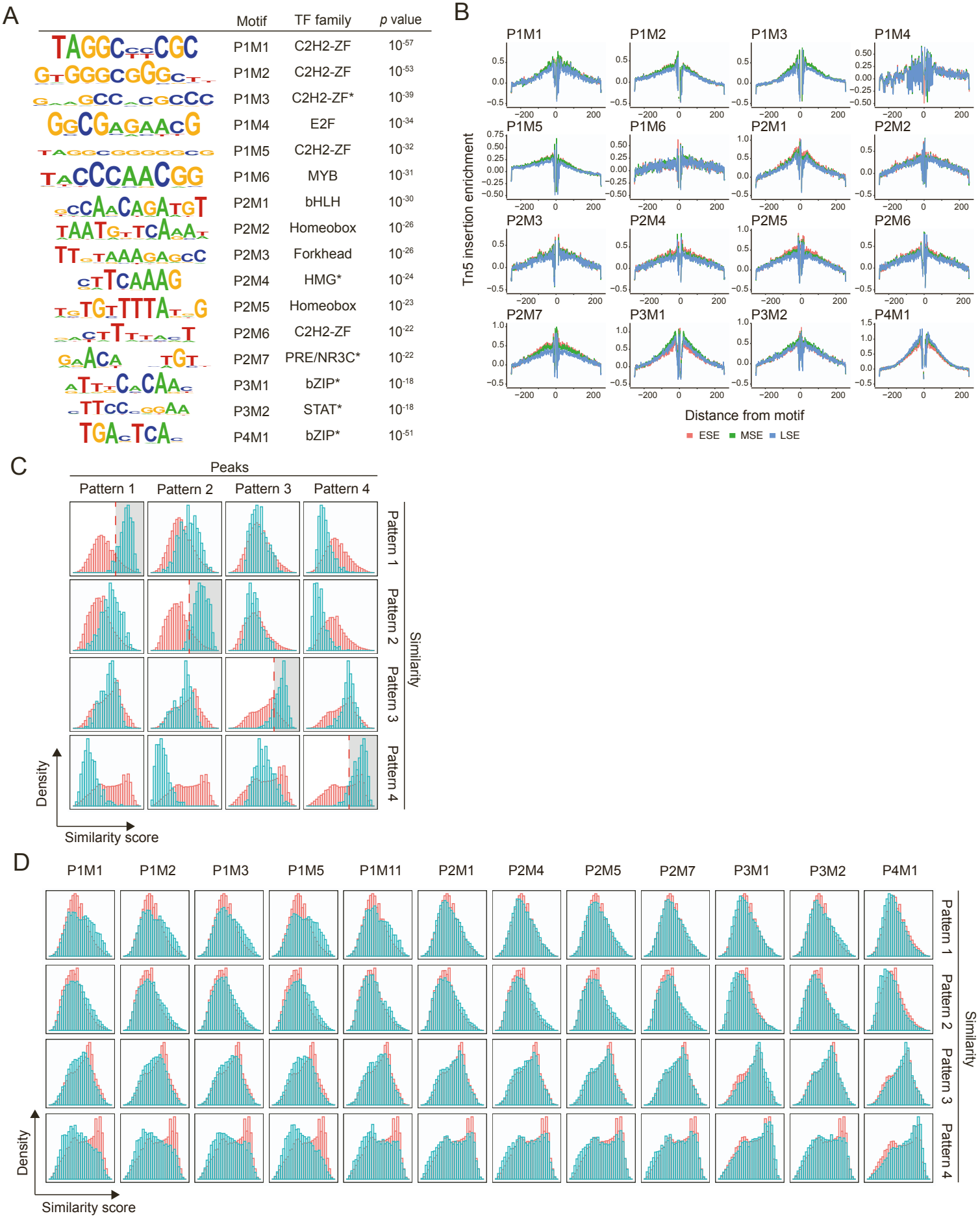

Figure S3, related to Figure 4. Enriched TF binding motifs in temporally regulated chromatin regions in decidualizing stromal cells.

(A) Table of enriched motifs. *P* values represent binomial test results using HOMER [S2]. Motifs shown are significantly enriched based on *p* value threshold determined by performing analysis 5 times on shuffled chromatin regions. Best TF family matches were based on known motifs in the HOMER motif database (Table S1C).

* indicates statistically significant TF family matches (FDR corrected *p* value < 0.05).

(B) Footprint analysis of temporally enriched motifs from panel A. Average transposase insertion centered around the motifs. Secretory samples were grouped as early-secretory endometrium (ESE; S18-19), mid-secretory endometrium (MSE; S20-21) or late-secretory endometrium (LSE; S22-25).
(C and D) All ATAC-seq peaks in decidualizing stromal cells scored according to their temporal pattern similarity.
(C) Validation of temporal pattern enrichment scores. Similarity cutoff point shown as dashed red line. Shaded areas indicate peaks in extended temporal pattern sets.
(D) ATAC-seq peaks grouped by presence of enriched motifs from panel A.

A

Ciliated EpC enriched motifs

Motif	TF family	*p* value
Ciliated M1	Rfx*	10^{-56}
Ciliated M2	C2H2-ZF	10^{-53}
Ciliated M3	E2F	10^{-49}
Ciliated M4	E2F	10^{-48}
Ciliated M5	ZBTB	10^{-46}
Unciliated M1	bHLH	10^{-86}
Unciliated M2	bZIP*	10^{-80}
Unciliated M3	bZIP	10^{-71}
Unciliated M4	SOX*	10^{-68}
Unciliated M5	Homeobox*	10^{-57}

B

Immune Cell Enriched Motifs

M over NK1,NK2 and NK3	Motif	TF family	*p* value
	M M1	ETS*	10^{-95}
	M M2	ETS	10^{-85}
	M M3	C2H2-ZF	10^{-61}
	M M4	C2H2-ZF	10^{-54}
	M M5	ETS*	10^{-54}
NK1, NK2 and NK3 over M			
	NK M1	ETS/RUNT*	10^{-57}
	NK M2	T-box	10^{-46}
	NK M3	RUNT	10^{-42}
NK1 over NK2 and NK3			
	NK1 M1	RUNT*	10^{-64}
	NK1 M2	RXR-like	10^{-45}
	NK1 M3	ETS/RUNT*	10^{-40}
	NK1 M4	ETS	10^{-36}
	NK1 M5	C2H2-ZF	10^{-33}

C

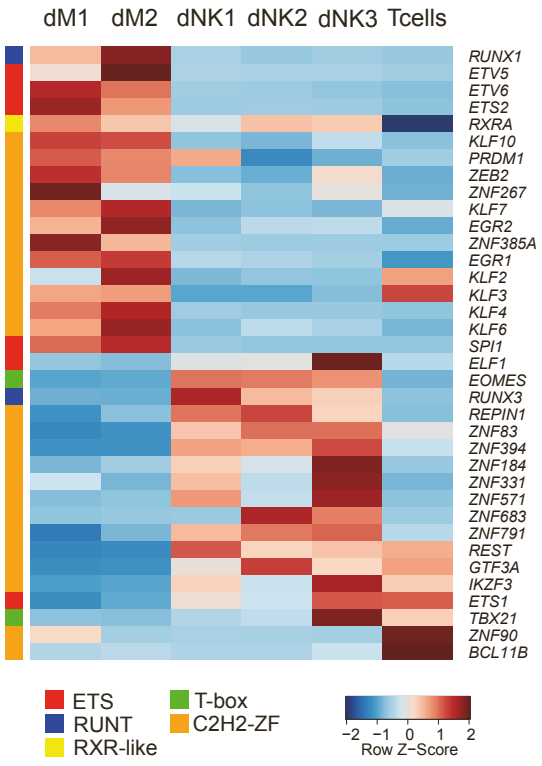

Figure S4, related to Figure 3 and Figure 6. Enriched TF binding motifs in ciliated epithelial and immune cells.

(A) Table of motifs enriched in ciliated and unciliated epithelial cells. Best TF family matches were based on known motifs in the HOMER motif database (Table S1C). * indicates statistically significant TF family matches (FDR corrected *p* value < 0.05).

(B) Table of enriched motifs in differential chromatin opening in immune cell subtypes. *P* values represent binomial test results using HOMER [S2]. Motifs shown are significantly enriched based on *p* value threshold determined by performing analysis 5 times on shuffled chromatin regions. Best TF family matches were based on known motifs in the HOMER motif database (Table S1C). * indicates statistically significant TF family matches (FDR corrected *p* value < 0.05).

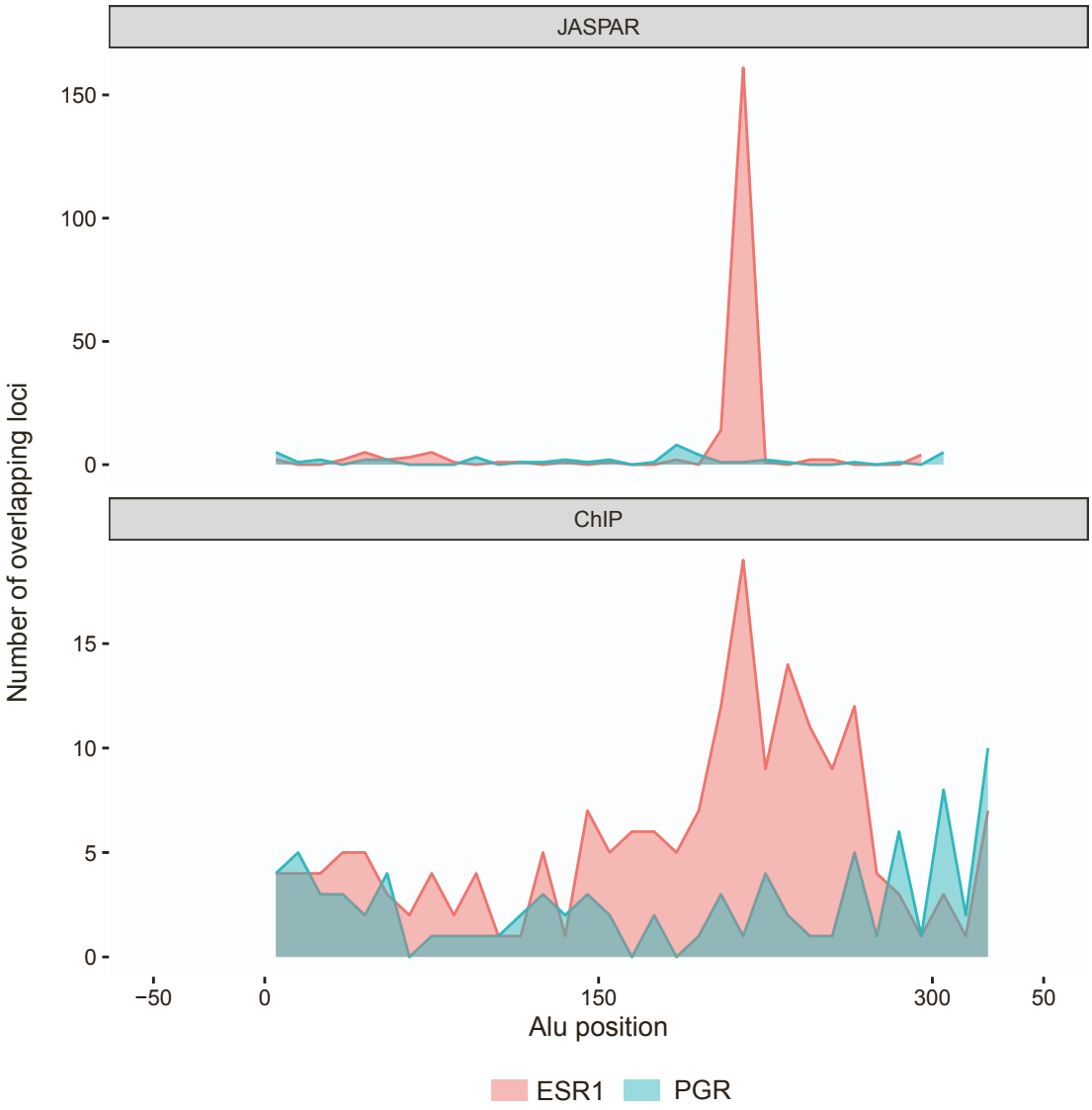

Figure S5, related to Figure 5. Density plots showing location of predicted and validated TFBSs from JASPAR database and ChIP-seq peak summits, respectively.

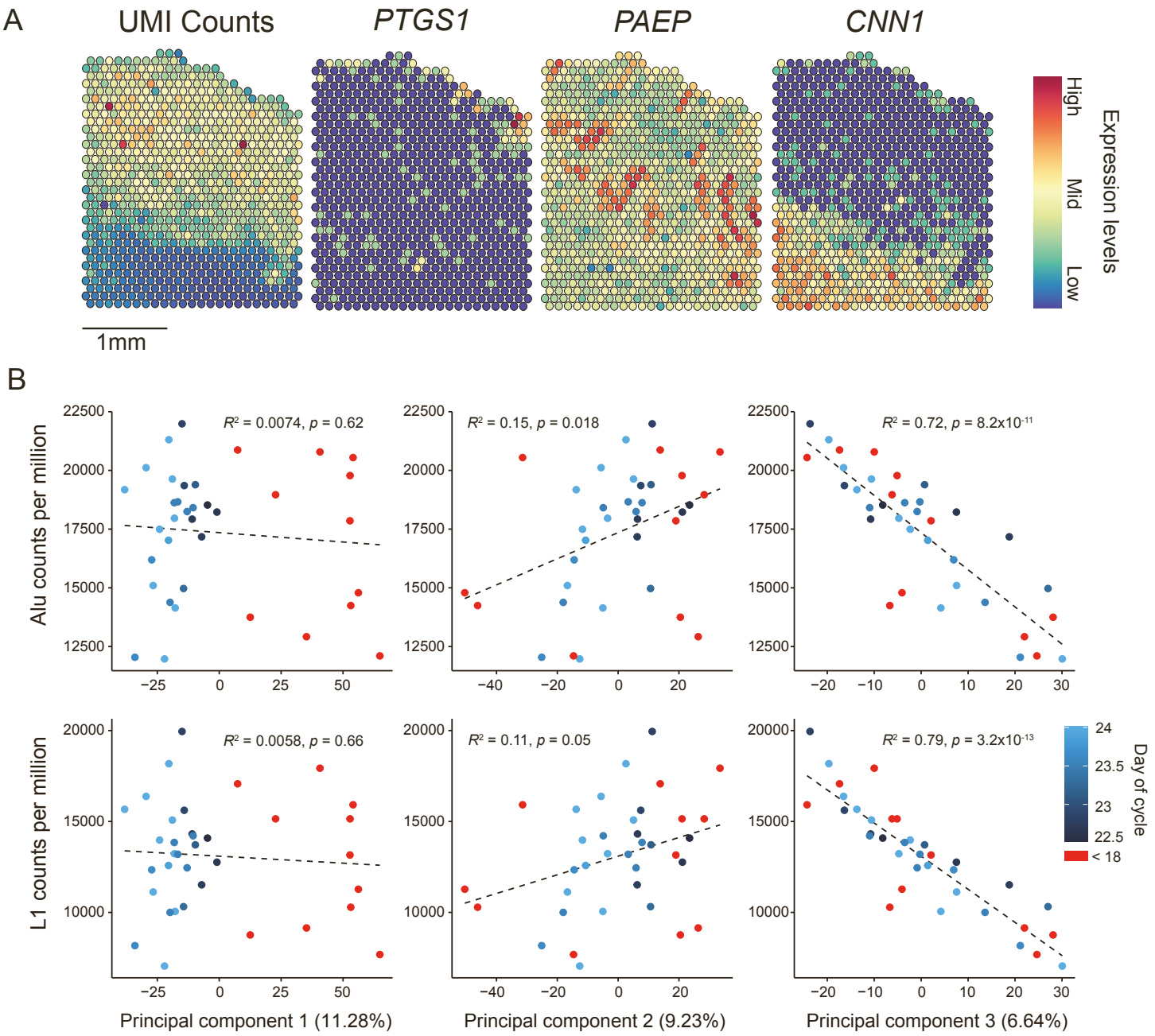

C

Alu and L1 enriched samples

Biological process	Enrich.	FDR
Ribosome assembly	12.75	2.37×10^{-11}
Regulation of programmed cell death	2.4	3.96×10^{-11}
Regulation of immune system process	1.93	6.65×10^{-5}
Cellular oxidant detoxification	5.46	8.48×10^{-4}
Positive regulation of natural killer cell	27.29	5.89×10^{-3}
Regulation of immune response	1.8	3.35×10^{-2}

Alu and L1 depleted samples

Biological process	Enrich.	FDR
Regulation of gene expression	1.82	1.07×10^{-17}
Signal transduction	1.47	8.25×10^{-6}
Chromatin organization	2.37	7.83×10^{-5}
Regulation of cell cycle	2.03	1.43×10^{-4}
Response to hormone	1.99	5.27×10^{-3}
Response to estradiol	3.73	1.41×10^{-2}

Figure S6, related to Figure 5. Alu and L1 RNA expression.
(A) Spatial transcriptomic results showing number of unique molecular identifier (UMI) counts and expression of marker genes: *PTGS1* (luminal epithelium and adjacent glands), *PAEP* (enriched in basal endometrial glands) and *CNN1* (myometrium).
(B) Correlation between Alu and L1 RNA expression with principal components (PC) in RNA-seq data obtained from 36 secretory phase endometrial samples [S3].
(C) GO analysis of top 500 PC3 genes in Alu and L1 mRNA enriched samples (left), and top 500 PC3 genes in Alu and L1mRNA depleted samples (right).

References

S1. Talbi, S., Hamilton, A.E., Vo, K.C., Tulac, S., Overgaard, M.T., Dosiou, C., Le Shay, N., Nezhat, C.N., Kempson, R., Lessey, B.A., et al. (2006). Molecular phenotyping of human endometrium distinguishes menstrual cycle phases and underlying biological processes in normo-ovulatory women. Endocrinology 147, 1097-1121. 10.1210/en.2005-1076.

S2. Heinz, S., Benner, C., Spann, N., Bertolino, E., Lin, Y.C., Laslo, P., Cheng, J.X., Murre, C., Singh, H., and Glass, C.K. (2010). Simple combinations of lineage-determining transcription factors prime cis-regulatory elements required for macrophage and B cell identities. Molecular cell 38, 576-589. 10.1016/j.molcel.2010.05.004.

S3. Lipecki, J., Mitchell, A.E., Muter, J., Lucas, E.S., Makwana, K., Fishwick, K., Odendaal, J., Hawkes, A., Vrljicak, P., Brosens, J.J., and Ott, S. (2022). EndoTime: non-categorical timing estimates for luteal endometrium. Hum Reprod 37, 747-761. 10.1093/humrep/deac006.